Dear Editor,

Please find below the point-by-point reply to the reviewer's comments (in italic) and our replies (preceded by "»"). The most relevant changes to the manuscript are a reconsidered presentation of the comparison with flux tower observations. We now isolate the spatial resolution effect in a first step and then compare MW and TIR ALEXI both at the lower resolution of MW data. We also removed the test of a simple combination of the two methods, as this does not improve it relative to this baseline and will need more thorough analysis. We also detailed the roadmap towards a combined MW and TIR ALEXI more clearly.

We look forward to hearing your opinion on this revised manuscript.

On behalf of all authors,

Thomas Holmes

Reviewer 1.

Intentionally, even if this is a MW based product, the authors have limited the analysis to the clear-sky estimates to facilitate the evaluation with the TIR estimates. I agree with this rationale, but I think the opportunity to already introduce some all-sky estimates in the tower evaluation was there. I suppose that even if there are some doubts about the boundary layer modelling for cloudy conditions, ALEXIS has been run for all available MW-LST Trads, so the ET outputs were available. If so, it would have been very interesting to see a tower evaluation of the 7-day totals of clear-sky ALEXI-TIR and ALEXI-MW, together with and ALEXI –MW 7-day totals but using all MW-Trad available. Presumably, estimating ET without the clear-sky restriction would have resulted in a better match to the tower observations, justifying all the trouble of developing a MW-based product. Given that using the MW Trad reduces the spatial resolution of the ET estimates by a factor of 5, there has to be some gain somewhere to justify their use.

I find adequate the level of description of ALEXIs in the text, but I'm missing some info about the concrete input datasets for this version of ALEXIS. Even if a paper presumably dealing with that is in review and cited in the text, at least the basic datasets to run ALEXIS in this global version should be given. The meteorology plays a crucial role in the derivation of the ALEXIS output, so I imagine that compared with the previous CONUS applications, something has been changed in that respect. A critical parameter there is the surface radiation, as the LST is also involved, and it may be of interest to know how the new LST data has been handle in that respect.

» We thank the reviewer for the helpful comments.

To the first question of why no preliminary investigating of all-sky estimates was included, the answer is that in this first-step paper we intentionally limited our scope to match the existing thermal-based ALEXI procedure. As a result, we did not process days that were flagged in the MODIS run, so we do not currently have an all-sky set available for this study. Investigation the behavior of ALEXI during more cloud covered conditions will be the topic of our future research. In terms of ET remote sensing, this paper is therefore a milestone along the way, not an end. In terms of MW-based LST remote sensing it is an important validation of independent information content compared to TIR products. The specific

scope of the paper is now more clearly described in the abstract and introduction, as well as critical follow-on steps.

We also note the request for more information on ALEXI input datasets. While all input sets to ALEXI are listed in Table 1, we will add information on shortwave incoming radiation, which was omitted in the discussion paper. And more information on the calculation of LW fluxes is now included in response to detailed questions below.

P1. L11. Given our current inability to properly validate global ET, I doubt that this exercise can be used to validate whether your diurnal temperature information from the MW obs is correct. You should show that your LST is reasonable before you attempt to estimate ET, as I think you did in previous publications, in which case there are no reasons for the ET to be unreasonable.
» In prior papers, we looked at temporal agreements between the satellite estimates and ground measurements from flux tower sites. What the analysis in this paper adds is a continental scale validation of the MW LST diurnal information using MODIS TIR LST. While the reviewer is correct that if the new LST inputs are reasonable, the ALEXI ET retrievals be reasonable, we move to the ET stage here to demonstrate sensitivity of this particular model to expected errors in the diurnal LST curve. The results show that the ET retrievals have some spatial differences that are explainable, but overall the TIR and MW ET estimates are sufficiently consistent under clear-sky conditions such that the next phases of investigation are warranted; namely evaluation of all-sky MW performance and development of a merged TIR-MW product.

P1. L25. The limitation to clear-sky estimates applies to those ET methodologies relying in TIR data, but there are already all-sky global ET estimates not depending that clearly on TIR data, perhaps "all-sky LST-based estimates"?
» We narrowed our statement to say: ".. towards all-sky satellite-based retrieval of ET through an energy balance framework".

P1. L28. The abstract should give information about the geographical coverage of the exercise, global?
» Indeed, 'global' is now added to the abstract (L17).

P3. L11. Most ALEXI applications have been restricted in the past to the CONUS. Now, that it is starting to reach other domains, I wonder if there are some thoughts regarding an estimation of rain interception by the canopy, which can have some importance at some regions.
» The effect of rain water, evaporated from the canopy before it reached the soil, will have a cooling effect on the composite radiometric temperature. We hypothesize that the interception loss will be incorporated into the total ET retrieval via SEB, but may indeed be mistakenly attributed in the soil evaporation residual term. This is something we plan to test over LBA and related flux sites using the MW-LST ALEXI retrievals. Since accurate partitioning of ET may be required for some applications, pending results we plan work on approaches for proper attribution of the interception component. However, we prefer that ALEXI remains a purely diagnostic model to maintain its role as independent estimate of ET, not requiring precipitation data as input. In the revised manuscript we make a note of this in the roadmap outlined in the discussion: "Finally, the all-sky implementation that is now within reach with ALEXI-MW will test the assumptions in new ways, which will require careful investigation. For example, the assumptions related to the boundary layer development may be tested as we move to include less stable conditions associated with cloudy skies. Similarly, evaporation of intercepted rain

water will feature more prominently under cloudy skies and may require inclusion as a separate process within the current physical framework.".

P3. L26. I think a few lines about the global implementation of ALEXI should be written. It is not clear if the global ALEXI is just plain ALEXI with global inputs, or something else has been changed. Also, what inputs ALEXI uses and the specific datasets are always interesting information. There are regions where Trad will have a very small impact on the ET estimates, i.e., there will be mainly driven by the meteorological data, so it is relevant to know about that data as well.
» The description of the ALEXI model (Section 2.1) is improved to more clearly state the two relevant differences between the global implementation and previous geostationary implementations: 1) MODIS based Trad, 2) operation on 7-day averages.

P3. L38. Is then the longwave heat loss recalculated with each temperature dataset? If so, how? I guess you need a daily integrated value for the Rnet, which is not straightforward as the LST datasets are not geostationary this time.
» Indeed, the LW heat loss is calculated in accordance with the temperature set that is used, using the Stephan-Boltzmann Law and a spatially varying emissivity. The ALEXI model computes the energy balance at two instantaneous points during the morning hours (post-dawn and pre-noon) using LST data available at those times. The latent heat estimate at the second time is then upscaled to a daily flux, conserving a flux ratio metric. In prior applications, we used available energy as the scaling flux, and that did require an estimate of hourly LWup (clear and cloudy). In this case, the model estimates of canopy and soil temperatures at time 2 were tied to the diurnal air temperature curve as described in Sec. 2.4 of Anderson et al. (2012). However, especially for global applications we find we get similar yet more robust and computationally less expensive results by scaling using the insolation flux. This bypasses the need for hourly Rnet/LST estimates.

This distinction is made more clear by stating that the Rnet is only calculated at time 1 and 2: "There are two pathways through which the T_rad input affects ALEXI ET estimates: through the estimation of the morning rise in temperature between time 1 and time 2, ΔT_rad, which affects the boundary layer growth and the strength of the sensible heat fluxes; and through the impact of TRAD on the upwelling longwave component of R_net at these times. "

Reference added: Anderson, M.C., Kustas, W.P., Alfieri, J.G., Hain, C.R., Prueger, J.H., Evett, S.R., Colaizzi, P.D., Howell, T.A., & Chavez, J.L. (2012). Mapping daily evapotranspiration at Landsat spatial scales during the BEAREX'08 field campaign. Adv. Water Resour., 50, 162-177

P4. L6. And when not over the GOES disk, how is MODIS LST converted to a Delta- Trad?
» We added a line to clarify this: "This regression model, trained over the GOES domain, is then applied globally to estimate Trad at time 1 and time 2 from MODIS LST."(Section 2.2)

P6. L1. It is not clear where the 7-day total comes from. I imagine there is a reason, linked to MODIS sampling (the MODIS ET product is 8-days). The meteorology can change quite significantly in 7 days, so if the 7-day total is based on one-day sampling, I can imagine that for some conditions the errors introduced can be large.
» The 7-day total comes from taking an average of all needed inputs on the "clear-sky" days in the 7-day period and running ALEXI. Based on the resulting "clear sky" ET, we calculate a ratio of instantaneous latent heat flux to incoming solar radiation (fSUN). This fSUN is held constant over the 7-day period and

used to calculate daily ET on each day, which is then summed to a 7-day total ET. This accounts for changes in atmospheric demand while preserving the evaporative fraction as determined on the clear-sky days. Running ALEXI on 7-day mean values was originally structured to limit computational demands and the system is currently being updated to produce daily simulations vs. the 7-day simulations used here. This information is added to Section 2.1 of the revised manuscript.

P6. L3. So the solar radiation is daily, and the ratio of ET to the radiation maintained constant for the 7-day period?
» This is correct. The daily solar radiation is used to account for changes in atmospheric demand while calculating the 7-day total ET (see response above).

P6. L11. What is the reason for the missing 31% MW estimates when there are TIR estimates? The spatial sampling of the MW product?
» We added the following explanation in the text in section 2.3.5: "The reason this percentage is not higher is mainly due to the requirement of a near-noon overpass for the fitting of the diurnal temperature curve (See Section 2.3.2), in combination with the 1 in 3 days without such overpass for a given location as determined by the orbit and coverage of Aqua and GCOM-W."

P6. L12. Why should the MW-LST being calibrated to MODIS-LST?
» We added the reason: ".. , something that is likely needed to maximize consistency between ALEXI implementations over the globe."(P6. L28.)

P6. L25. Do you use the energy closure corrected fluxes or the original ones?
» This analysis made use of the gapfilled ones (LE_F_MDS), not the energy closure corrected fluxes, and is now specified in section 2.4.

P6. L30. This is a bit confusing, even if discussed already in Section 2.3. If only in Africa and Europe the scaling of MW-LST supported, but you have then MW-LST globally, and presumably the ET, how "bad" is the MW-LST and ET outside those regions? Or, in other words, can we globally use the MW-LST ET or we need to wait for further developments in the MW-LST calibration outside those regions?
» At the end of the revised paper (p12 L9) we present the roadmap for global all-sky ET. The first step being: a global observation based calibration of MW-LST with MODIS-LST to reduce biases as identified at the high incidence angles of the MSG domain and avoid the need for extrapolation of scaling parameters.

P7. L15 14 mm/month) THAN? Then?
» Corrected.

P7. L18. I guess that's the grey color in Figure 4. It should be mentioned in the figure caption.
» We added to the caption of Figure 4: '. …with areas with ET below 14 mm/month greyed out.'

P8. L1. Have you found any explanations for the lack of agreement in the Horn of Africa? Trad seems to agree relatively well.
» The MW ΔTrad is a little bit lower than the TIR estimate, whereas the MW ET is much higher than the TIR estimate. The opposite signs are in agreement, but the response is larger than in other arid regions, like the Northern Sahel. We don't have an explanation for this higher sensitivity in this region at this point, but this is something we will be investigating. We hypothesize that the model be encountering a threshold condition in this region (e.g., running up against the constraint that throttles back the canopy

transpiration when negative midday soil evaporation is obtained). This would make the model hypersensitive to small changes in DT in these areas.

P8. L32. I'm surprised by a large part of France being masked by the grey color, i.e., not showing inter-annual variability. Most of the other grey areas are in the very dry regions, as expected, which is not the case of France.
» Upon closer look at the creation of this figure an error was found in the processing. The figure in the original manuscript represent correlation in cumulative anomaly, not anomaly in 3-month totals. The new figures reflect the actual 1-month and 3-month cumulation of anomalies. And this indeed reveals France, as the reviewer expected it should.

P9. L14. Yes, very counterintuitive result and a bit worrying regarding the quality of these metrics. What do you mean by spatially uncorrelated noise? What MODIS? LST or the ET? This is not clear to me, it may be worth explaining better if you think you know the causes of this behavior.
» The sentence itself (*P9. L33*) can be clarified to answer some of these questions: "This indicates the presence of spatially uncorrelated noise in the 0.05° MODIS LST input that is uncorrelated with the surrounding 0.25° grid average and negates any positive effect of its resolution advantage compared to a 0.25° grid average for most sites. ". It may be that the selected sites are in relatively homogeneous terrain in terms of ET, in which case statistics may be improved by averaging more pixels. It is clear though, that this is an issue that plays in the averaging from 0.05 to 0.25 ET retrievals. In the revised manuscript, we will split this out more clearly from the comparison between MW and TIR ET retrievals by using the 0.25 degree TIR-ET as the reference. This raises the bar a little bit for MW ET in terms of correlation but has the same RMSE.

P9. L20. What about the GOES-based time-extrapolation of the MODIS-LST to obtain Trad, can we see something here?
» It seems more obvious that the overwhelming difference is between more humid climates represented in the MSG domain as opposed to the GOES domain. As the number of datasets is too small to split them out by both domain and climate we cannot investigate the effect of calibration domain further.

P9. L21. with AN alpha is?
» Changed to 'an alpha parameter of 1.26'

P9. L24. Water limited regions are where Trad has a larger impact on the ET estimates. This suggests that ALEXI operates better when the ET depends less on Trad, right?
» Yes, in an extreme case, the humid tropics, the ALEXI ET is entirely driven by evaporative demand as parameterized with Priestly Taylor, with no impact of Trad. This is noted in Section 3.3. This is typically the case with most TIR-based ET models – when conditions are closer to potential, the model tends to perform better.

P10. L13. I think this needs a bit more of elaboration. Why do we want to merge both estimates? What is the overall strategy? The landscape is something that we cannot change, do you mean merging only when the landscape is homogeneous? But surely, merging spatial estimates at different resolutions will require up-scaling of the finest resolution one, or am I missing something?
» I think the wording was not clear here. We changed to simply say: "The above analysis of flux tower

data suggests that the prospect for merging MW and TIR is good for humid climate regions in general. In arid climates…" The overall strategy is outlined at the end of the conclusion.

P10. L15. I think is a bit too simplistic to just blame signal to noise ratio in arid regions as the reason for the poorer performance of ALEXIS there. Deriving the accurate stress needed for the water limited regions is where current ET methodologies, independent of modeling framework, tend to struggle, and ALEXI does not seem to be an exception here.
» Signal to noise may indeed be only part of the explanation. We changed the sentence (start of 3.5) to: "Partly, this reflects a lower signal to noise in areas with low seasonal variation in ET, but it also reflects a more challenging environment for ALEXI with little vegetation. "

P11. L15. Why is this result surprising? If the MW-LST and TIR-LST are reasonable estimations of the true LST, and the rest of the ALEXIS modeling and inputs are unchanged, I will not expect large differences between both ALEXIs.
» We removed the word 'surprisingly' and leave it to the reader to be surprised, or not.

P11. L24. I would agree if ALEXI were using raw MW-LST and TIR-LST observations. But the MW-LST has been fitted to the TIR-LST, so I am not sure the independence is that obvious as stated in the text.
» The mapping of MW brightness temperature to LST is based on 4 time-constant maps of fitting parameters – there is no transfer of temporal information from TIR-LST to MW-LST.

P11. L27. The improvement is 0.02, very modest, and it is obtained by combining estimates of different resolution, with one of them covering an area 5 times larger than the other. Given the discussion of the spatial degradation helping to improve correlations, I'm not sure we are just dealing with independence of datasets.
» We agree that there may be more factors at play with this limited set of flux towers. The sentence (P12. L6) is changed to a less strong wording: "The overall observed improvement from ρ=0.76 to ρ=0.78 confirms is in agreement with an expectation that part of the error in ET estimates from ALEXI-IR and ALEXI-MW is independent. "

P11. L30. So far, all this is clear-sky. I suppose that MW-LST will be used always, not only for clear-sky, and that some work may be needed to see whether the assumptions of boundary layer development work for all-weather conditions. If so, it may be worth adding to this short roadmap.
» Indeed, this was an omission in our roadmap. We added a few lines in the conclusion: "Finally, the all-sky implementation that is now within reach with ALEXI-MW will test the assumptions in new ways, which will require careful investigation. For example, the assumptions related to the boundary layer development may be tested as we move to include less stable conditions associated with cloudy skies. Similarly, evaporation of intercepted rain water will feature more prominently under cloudy skies and may require inclusion as a separate process within the current physical framework.".

Reviewer 2.

The authors have used diurnal temperature cycle built on available MW sensors to the well-known ALEXI model. The quality of diurnal temperature cycle based on MW sensors is important to ET retrieval. LSA-SAF LST was used to calibrate MW LST.

I am wondering how did they determine or scale MW DTC parameters (especially the diurnal amplitude A) for the regions outside of SEVIRI coverage? Does MODIS ALEXI IR also use LSA-SAF LST to determine DTC parameters? I am confusing with eq. 1 and eq. 2 and 3. A_MW can be derived with equation 1. The diurnal cycle can then be produced with DTC3 model. eq. 2 says A_MW is scaled with TIR-based parameters. Then shouldn't the diurnal temperature cycle will also be changed by the new A_MW? When A_MW equals A_IR, shouldn't dTrad_IR and dTrad_MW be the same or very close? Then ET_MW and ET_IR will certainly have a high correlation. Please compare with other ET dataset, such as the latitudinal transect in Fig. 6, Fig. 7, Fig. 9. Otherwise, comparison between ALEXI_IR and ALEXI_MW is not enough for evaluation of the method.

In addition, when they evaluate the ET results with Fluxnet, please do the analysis on a daily scale. A part of the purpose using MW here should be also providing ET at daily scale. So please assess the daily ET not weekly or monthly.

» Thank you for the comments and reflection on the manuscript. In response to these general comments we want to stress that:

- Only the long term mean of the diurnal parameters is scaled to match those of LSA SAF TIR. The entire transfer of information from TIR to MW is contained in three static maps (for amplitude, mean, and timing). This means that the correlation between the diurnal amplitudes of TIR and MW LST is not affected – in terms of short-scale inter-seasonal patterns the two sets remain independent.

This point is now emphasized in the description of Eq2-3 and the process of creating MW-LST:

Section 2.3.3: "Because all three parameters are constant with time, Eqs 2-3 preserve their temporal independence of the TIR LST product."

- For the extrapolation of MW to LSA-SAF LST calibration parameters outside the Meteosat domain we used ad-hoc linear regressions with vegetation characteristics (MW vegetation optical depth). It is not an approach we will continue with. For this paper, we use it to bring the dataset in the approximate range of the TIR LST, but only to include it in the analysis of temporal signal with Fluxnet data. Again, the temporal signal is not affected by the calibration.

In light of this, we do think a comparison between MW and TIR ALEXI is a valid test of performance at this point and a strong indication of diurnal information content in MW LST.

I am wondering why don't they use MW and IR signal to build diurnal temperature cycle directly. Could this method get more accurate daily global ET? Xuelong Chen has found MODIS monthly LST products could capture the monthly mean of diurnal LST variation. This means that the ALEXI could be used to MODIS monthly LST products. The authors might be interested to the following figure 1.

» It is certainly possible that we will eventually merge MW and IR to get a better estimate of diurnal temperature. However, this still requires some additional steps to overcome, not least of which is the

spatial resolution difference. This paper presents a milestone along the way, reporting on an experiment to test MW LST in an ET retrieval that is itself sensitive to the diurnal information.

Eq1. If possible, please give the equation of DTC3, then the readers could quickly understand what kind of curves were used to fit the diurnal cycle.

» We added the description of the DTC model as a model that " combines a cosine and an exponential term to describe the effect of the sun and the decrease of surface temperature at night". We think that this level of detail is sufficient for understanding the present paper, and listing the exact equations might distract from the main analysis. For a detailed description, the reader is referred to Holmes et al 2015 and references therein.

Section 2.3.2 now includes this passage: "The DTC model combines a cosine and an exponential term to describe the effect of the sun and the decrease of surface temperature at night and is based on Göttsche and Olesen (2001) with slight adaptations to limit the number of parameters. This implementation (DTC3) is fully described in Holmes et al. (2015). "

Fig. 4 please specify t1 and t2 time for dTrad.

» We added to the caption: dTrad is defined in the ALEXI framework as the temperature rise between 1.5 hr after sunrise to 1.5 hr before noon (see Section 2.1).

Fig. 8 how did the authors cope with different spatial resolution when they calculate Pearson's correlation. ALEXI-IR is 0.05 deg and ALEXI-MW is 0.25 deg. The correlation is at 0.05 deg resolution?

» The correlation in 3-month anomalies (Fig 8) is calculated based on 0.25 degree resolution data. This is now specified in the caption.

Fig. 9 why not calculate monthly anomaly? MW provide the possibility of daily ET. 3 months anomaly will provide more consistent spatial patterns. But the performance at daily or monthly is more interesting. Fig. 7, and 8 also have the same question.

» 3-month anomalies were chosen to represent the larger seasonal patterns in interannual variation. Higher temporal resolution is tested with in situ data's. As can be seen in the below figures, the correlations are rather similar between the 1-month and 3-month anomalies.

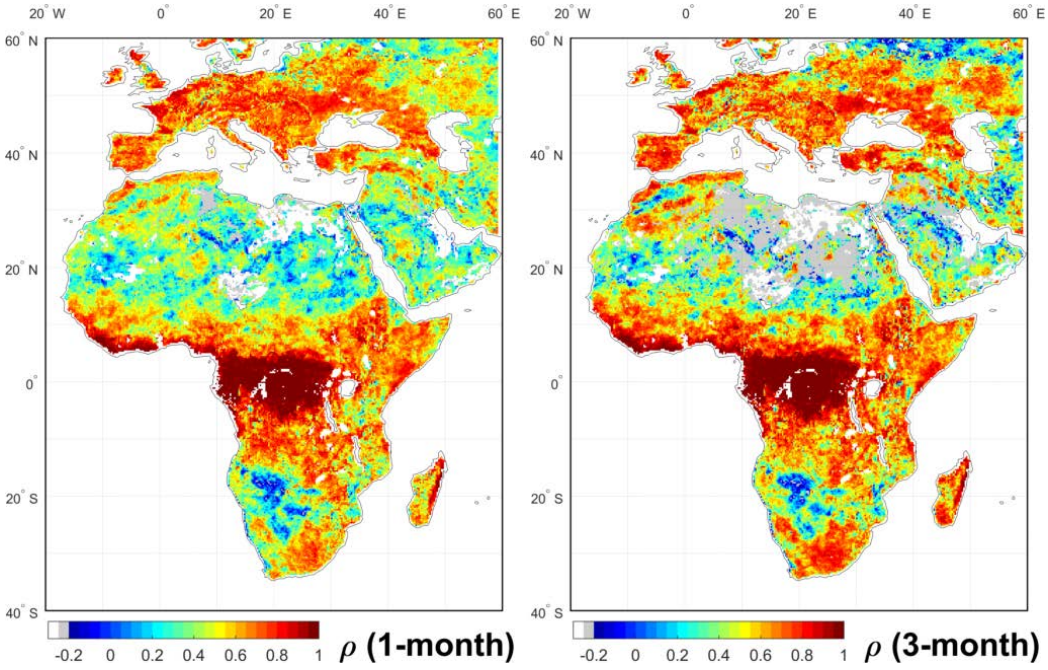

Figure 1: Pearson's correlation between anomaly in 1-month (left) and 3-month (right) ET totals as estimated by ALEXI-IR and ALEXI-MW, calculated at 0.25 degree resolution. White areas have no data, grey areas are masked because the standard deviation in in anomaly was below 2.5 mm/month in both estimates.

Figure. 10, when you calculate pearson correlation between satellite data and Fluxnet observations, daily, weekly, or monthly time series data was used? Please give RMSE at mm/day. This is more comparable to other's result.

» Thanks for pointing this out, the caption did not specify that these statistics are based on weekly ET values. For ALEXI these weekly values are interpolated from clearsky observations as detailed in Section 2.4. The Fig 10 caption is changed to start with: "Comparison of Pearson correlation (rho) and RMSE between estimates of weekly ET from satellite data and Fluxnet observations."

Describe what is ti in Equation 1.

» The definition of t is given in the preceding sentence, 'ti' is the observation time of the temperature measurement. The index 'i' is used to represent the individual observations within a day.

Table 2 Comparison is based on weekly averages in the period of 2003 to 2011. Why not use daily ET with gaps to calculate R, RMS? This is more useful for the readers to compare other ET products. Surely, weekly averages will give a higher R and low RMS. But MW provide ALEXI with the possibility for daily ET calculation. AND page 2, 'generated a data record of weekly ET' why not daily? as above comments \

» While the goal of this work is to eventually reduce the temporal interval of consistent ET retrievals to daily, at this moment we followed the existing global ALEXI protocol that allows for evaluation of weekly ET totals. We do look forward to analyzing daily output in future studies, but it was not an option at this stage of the development.

Table 1, MOD43C3 doesn't have gaps? How did they fill albedo gaps? Please specify at what time step (00:00, 06:00: : :) lapse rate profile is used.

» In fact, it should have read MCD43B3 and this is a 16-day product. The updated reference (Schaaf et al. 2002) explains: ".. BRDF parameters are produced (via either full or magnitude inversions) for every land or coastal area which is viewed (and atmospherically corrected) at least once over a 16-day period. Land areas that remain completely cloud covered over this period are designated with fill values."

Schaaf, C. B., Gao, F., Strahler, A. H., Lucht, W., Li, X., Tsang, T., Strugnell, N. C., Zhang, X., Jin, Y., Muller, J.-P., Lewis, P., Barnsley, M., Hobson, P., Disney, M., Roberts, G., Dunderdale, M., Doll, C., d'Entremont, R. P., Hu, B., Liang, S., Privette, J. L. and Roy, D.: First operational BRDF, albedo nadir reflectance products from MODIS, Remote Sens. Environ., 83(1–2), 135–148, doi:10.1016/S0034-4257(02)00091-3, 2002.

Microwave implementation of two-source energy balance approach for estimating evapotranspiration

Thomas R. Holmes[1], Christopher Hain[2], Wade T. Crow[3], Martha C. Anderson[3], William P. Kustas[3]

[1]Hydrologcal Sciences Lab, NASA Goddard Space Flight Center, Greenbelt, MD, 20771, USA
[2]Earth Science Office, NASA Marshall Space Flight Center, Huntsville, AL, USA
[3]Hydrology and Remote Sensing Laboratory, USDA-ARS, Beltsville, MD 20705, USA

Correspondence to: Thomas R. Holmes (thomas.r.holmes@nasa.gov)

Abstract. A newly developed microwave (MW) land surface temperature (LST) product is used to substitute thermal infrared (TIR) based LST in the Atmosphere Land Exchange Inverse (ALEXI) modelling framework~~two source energy balance approach (TSEB)~~ for estimating ET from space. ALEXI implements a two-source energy balance~~This~~ (TSEB) land surface scheme in a time-differential approach, ~~, the Atmosphere Land Exchange Inverse (ALEXI) model framework, is an approach that minimizes~~designed to minimize sensitivity to absolute biases in input records of LST through the analysis of the rate of temperature change in the morning. Thermal infrared (TIR) retrievals of the diurnal LST curve, traditionally from geostationary platforms, are hindered by cloud cover, reducing model coverage on any given day. This study tests the utility of diurnal temperature information retrieved ~~This experiment is therefore an important test of the ability to retrieve diurnal temperature information~~ from a constellation of satellites with microwave radiometers that together provide 6-8 observations of Ka-band brightness temperature per location per day. This represents the first ever attempt at a global implementation of ALEXI with MW-based LST and is intended as the first step towards providing all-weather capability to the ALEXI framework. ~~The leveraging of all sky capability of MW sensors is the main motivation of this work, as TIR based ALEXI is limited to clear sky conditions.~~

The analysis is based on ~~a~~ 9-year long, global records of ALEXI ET generated ~~with~~ using both MW ~~LST~~ and TIR based diurnal LST information as ~~an~~ input~~, which is compared to an existing implementation of the same framework with thermal infrared based LST~~. In this study, the MW-LST sampling is restricted to the same clear sky days as in the IR-based implementation to be able to analyse the impact of changing the LST dataset separately from the impact of sampling all-sky conditions. The results show that long-term bulk ET estimates from both LST sources agree well, with a spatial correlation of 92% for total ET in the Europe/Africa domain and agreement in seasonal (3-month) totals of 83-97 % depending on the time of year. Most importantly, the ALEXI-MW also matches ALEXI-IR very closely in terms of 3-month inter-annual anomalies, demonstrating its ability to capture the development and extent of drought conditions. ~~The w~~Weekly ET output from the two parallel ALEXI implementations is further compared to a common ground measured reference provided by the FLUXNET consortium. Overall, the two model implementations generate ~~they indicate a surprisingly close match in both~~similar performance metrics (correlation and RMSE) for all but the most challenging sites in terms of spatial heterogeneity and level of aridity. It is concluded that a constellation of MW satellites can effectively be used to provide LST for estimating ET through ~~TSEB~~ALEXI, which is an important step towards all-sky -satellite-based retrieval of ET ~~estimates through~~using an energy balance framework.

1 Introduction

Estimating terrestrial evapotranspiration (ET) at continental to global scales is central to understanding the partitioning of energy and water at the earth surface and for evaluating modelled feedbacks operating between the atmosphere and biosphere. ET is an important flux that links the water, carbon, and energy cycles (Campbell and Norman, 1998). Approximately two-thirds of the precipitation over land is returned to the atmosphere by ET (Baumgartner & Reichel, 1975). Moreover, ET consumes 25-30% of the net radiation reaching the land surface (Trenberth et al., 2009). ET occurs as a result of atmospheric demand for water vapor and

depends on the availability of water and energy. When plants are present, this balancing is controlled by leaf-level stomatal controls, and in agricultural areas the water availability may also be managed at the field scale through irrigation or drainage. The high spatial and temporal variability in the driving mechanisms in combination with possible field-scale management decisions poses a significant challenge to bottom-up modelling of ET at sub-monthly time scales, even at the spatial scales of numerical weather prediction (NWP) models (5-25 km). In order for NWP models to improve the characterization of the surface energy budget, there is a need for timely diagnostic information on ET (Hain et al., 2015). This, in turn, could lead to a more timely and accurate identification of developing droughts (Anderson, 2011) which would aid farm-level management decisions as well as regional yield impact predictions.

ET is highly variable in space, so no amount of ground stations can provide an accurate estimate of the spatial average over larger domains, let alone the globe. Therefore, approaches have been developed to integrate satellite data with models to estimate ET from space. Surface energy balance approaches use surface temperature observations as the main diagnostic to estimate ET by partitioning the available energy into turbulent fluxes of sensible heating (H) and latent heating (LE). In the two source energy balance (TSEB) approach (Kustas and Norman, 1999; Norman et al., 1995) the partitioning is evaluated for the soil and the canopy separately. Anderson et al (1997) modified TSEB to leverage observations of the time evolution of surface temperature as a way to reduce the impact of biases in instantaneous temperature observations on the ET retrieval. This approach allowed for regional implementation of TSEB and came to be known as the Atmosphere Land Inverse Exchange (ALEXI) method (Anderson et al., 2007a; Mecikalski et al., 1999).

To date, ALEXI has always been implemented with land surface temperature (LST) retrievals from thermal infrared (TIR) imaging radiometers (Anderson et al., 2011). Most applications of ALEXI have utilized data products from geostationary satellites, for example the Geostationary Operational Environmental Satellite (GOES) with coverage over the Americas. More recently it has been applied to records from polar orbiting satellites to obtain consistent global coverage from a single sensor with short latency. This is based on day-night temperature differences from the Moderate Resolution Imaging Spectroradiometer (MODIS) on the Aqua satellite from NASA's Earth Observing System (EOS) program (Hain and Anderson, in press). Reliance on TIR effectively limits ~~surface observations~~ET retrievals to clear skies (Rossow et al., 1989), and failure to completely mask cloud affected observations is shown to limit the precision in TIR-LST (Holmes et al., 2016). Continuous daily estimates of ET are generated from clear-sky ALEXI samples through temporal interpolation based on maintaining a normalized flux partitioning metric. In ALEXI this also accounts for daily evaporative losses (Anderson et al., 2007a). Recent work by Alfieri et al. (2017) analysed measurements from eddy-covariance towers and found the persistence for energy flux partitioning metrics to be short. In their analysis, they found that a return interval of no more than 5 days is necessary to keep the relative error in daily ET below 20 %.

In order to provide a more consistent and short return interval for daily ET ~~measurements~~retrievals at the global scale there is a need for accurate values during cloudy intervals. The approach we take here to address this challenge is to leverage passive microwave (MW) observations. The longer wavelengths (0.1-1 m) make MW observations of the land surface generally less susceptible to scattering and absorption by clouds than observations in the TIR spectral region (except for notable water and oxygen absorption windows; Ulaby et al. (1986)). One MW frequency band with a particularly high sensitivity to LST (Prigent et al., 2016) and high tolerance to clouds (Holmes et al., 2016) is Ka-band (36-37 GHz). MW radiometers with a Ka-band channel are available from several low Earth orbiting satellites that sample at different times of the day. ~~Together~~ Collectively they can be used to construct a diurnal cycle of brightness temperature for each location on Earth (Holmes et al., 2013b; Norouzi et al., 2012). This diurnal brightness temperature can then be scaled to match the diurnal temperature cycle as measured by TIR imagers (Holmes et al., 2015, 2016).

The methodology developed in Holmes et al (2015) was applied to create an 11-year record of MW-based LST (MW-LST) from various Ka-band sensors (See Section 2). Because this new dataset specifically includes diurnal information, it presents an

opportunity to evaluate use of constellation-based MW-LST in a TSEB framework for estimating ET. For this purpose, we substituted MW-LST for MODIS LST in the global implementation of ALEXI as described in Hain and Anderson (in press) and generated a data record of weekly ET for the time-period 2003 to 2013 using each LST data source. No re-calibration of ALEXI was applied in this experiment to accommodate MW-LST. The only difference between the two resulting multi-year records of ET estimates are the spectral window (MW Ka-band ~~Vs~~ vs. TIR) and spatial resolution of the LST inputs (0.25° for the MW implementation: ALEXI-MW, and 0.05° for the MODIS implementation: ALEXI-IR). In order to make the subsequent comparison with ALEXI-IR as direct as possible, the MODIS cloud mask was also applied to MW-LST. This assures that potential issues related to the applicability of the ALEXI framework during cloudy conditions (particularly its assumptions regarding boundary layer development) are separated from the question of MW-LST performance within the two-source framework. The results are discussed by region and season, and in terms of bulk ET and its inter-annual variation. With this analysis, we hope to establish the degree to which ALEXI-MW resembles the ALEXI-IR ~~in~~ under clear sky situations. The performance of the ALEXI model with all-sky LST observations will be the topic of subsequent investigations.

2 Methodology

2.1 ALEXI model

The ALEXI method is a comprehensive set of algorithms to diagnose the surface energy balance with the aim of retrieving ET (Anderson et al., 2007a; Mecikalski et al., 1999). ALEXI~~It~~ is based on the TSEB ~~approach~~ land-surface parameterization (Kustas and Norman, 1999; Norman et al., 1995) in which the partitioning of turbulent fluxes is evaluated for the soil (s) and the canopy (c) separately. This is accomplished by 1) ~~parameterizing~~ partitioning the ~~divergence of~~bulk net radiation (*Rnet*) between canopy and soil surface components and 2) attributing the observed composite surface radiometric temperature (*Trad*) ~~in~~to soil and canopy temperatures, T_s and T_c based on vegetation cover fraction. An initial guess for the ~~canopy transpiration~~canopy latent heat is based on the assumption that the green part of the canopy transpires at its potential rate ($LE_c = LE_{PT}$), where LE_{PT} is estimated with a modified Priestley and Taylor approximation (1972). The sensible heat flux for the two source components (H_s and H_c) is then calculated in a set of equations that accounts for their different resistance to heat transfer and that satisfy the observation-based T_s and T_c and air temperature T_a (Norman et al., 1995). The final estimate of ~~ET~~ latent heat is determined in an iterative procedure in which LE_c is reduced until a solution is found where the soil evaporation (LE_s) is non-negative. ET (in units of mass flux) is computed from the latent heat (units of energy flux) by dividing by the latent heat of vaporization.

ALEXI couples TSEB with an atmospheric boundary layer model to relate the morning rise in T_{rad} ~~*Trad*~~ to the growth of the overlying planetary boundary layer and simulate an internally consistent T_a. This removes the need for T_a as an input dataset and limits the sensitivity of the method to biases in instantaneous satellite-based temperature estimates, while allowing for regional and global implementations of the model (Anderson et al., 1997). The ALEXI model is intended for ~~large~~ coarse spatial grids (~5 km ~~grids~~pixels) and provides the physical foundation to the multi-scale ALEXI/DisALEXI modelling system that has been applied to many satellite-based TIR data streams from 30-m to 10-km spatial resolutions (Anderson et al., 2011). The primary input to ALEXI is T_{rad} at two times during the morning: 1.5 hours after sunrise (time 1) and 1.5 hours before solar noon (time 2). There are two pathways through which the T_{rad} input affects ALEXI ET estimates: through the estimation of the morning rise in temperature between time 1 and time 2, ΔT_{rad}, which affects the boundary layer growth and the strength of the sensible heat fluxes; and through the impact of T_{rad} on the upwelling longwave component of R_{net} at these times. Whereas the former is not sensitive to time-invariant biases in the diurnal temperature retrievals, the latter has a weak sensitivity to the absolute temperature at time 1 and time 2.

The experiment described in this paper is based on a recent global implementation of the ALEXI model (Hain and Anderson, in press). This global ALEXI implementation differs from prior geostationary implementations in that its analysis is performed at weekly timescales. In practice this means taking an average of all needed inputs on the "clear-sky" days in the 7-day period and running ALEXI. Based on the resulting "clear sky" ET, we calculate a ratio of instantaneous latent heat flux to incoming solar radiation (fSUN). This fSUN is held constant over the 7-day period and used to calculate daily ET on each day, which is then summed to a 7-day total ET. This accounts for changes in atmospheric demand while preserving the evaporative fraction as determined on the clear-sky days. While a daily system is in preparation, at present, the global model is executed using 7-day averages of all inputs to minimize computational load. ET outputs are also reported in units of 7-day total ET, or mm/week. The data sources for this version of ALEXI are listed in Table 1. ~~The primary input to ALEXI is T_{rad} at two times during the morning: 1.5 hours after sunrise (time 1) and 1.5 hours before solar noon (time 2).~~ This paper compares two sets of ALEXI ET estimates based on the exact same global model formulation but with alternative LST inputs ~~used~~ to estimate the time integrated change in mid-morning T_{rad}. The baseline is a TIR version that makes use of MODIS-LST from the Moderate Resolution Imaging Spectroradiometer (MODIS) on the polar orbiting satellites Aqua and Terra from NASA's Earth Observing System (EOS) program. This MODIS-based T_{rad} estimates are~~, which is~~ used as the input in the current global ALEXI implementation (Hain and Anderson, in press) described in Section 2.2. The alternative LST input from MW data is described in Section 2.3. The two separate implementations of ALEXI are identified by their temperature input source: ALEXI-IR (with MODIS-LST) and ALEXI-MW (with MW-LST). A~~, a~~ll other inputs needed to run ALEXI are identical for both implementations.

~~There are two pathways through which T_{rad} affects ALEXI ET estimates: directly through the estimation of the morning rise in temperature, ΔT_{rad}, which affects the boundary layer growth and the strength of the sensible heat fluxes; and through the impact of TRAD on the upwelling longwave component of RNET at these times. indirectly through the calculation of the longwave heat loss, both at the canopy and at the soil surface, which factors in *Rnet*. Whereas the former is not sensitive to time invariant biases in mean daily temperature~~the diurnal temperature retrievals~~, the latter has a weak sensitivity to the absolute temperature at time 1 and time 2. While a daily system is in preparation, at present, the global model is executed using 7-day averages of all inputs to minimize computational load. ET outputs used here are reported in units of 7-day total ET, or mm/week~~

2.2 Temperature from MODIS

The MODIS instrument on the polar-orbiting Aqua satellite (July 2002 to present) with an equator overpass time of 1:30 a.m. / p.m. provides global TIR observations with spectral bands suitable for estimating LST. The specific LST product used for the ALEXI implementation is the MODIS Climate Modelling Grid (CMG) 0.05° daily LST product (MYD11C1 (Wan, 2008)), which is distributed by the Land Processes Distributed Active Archive Center (https://lpdaac.usgs.gov). Although the overpass times of this satellite do not correspond directly with ALEXI's time 1 and time 2, Hain et al. (2017) show that over the U.S., GOES-based ΔT_{rad} can be estimated with a 5-10 % relative error using a tree-based regression model based on independent variables including vegetation index, and landcover class. This regression model, trained over the GOES domain, is then applied globally to estimate T_{rad} at time 1 and time 2 from MODIS LST.

2.3 Temperature from a constellation of MW satellites

The MW-LST product is based on vertical polarized Ka-band (36-37 GHz) brightness temperature (T^{Ka}), a spectral band commonly included in multi-frequency microwave radiometers in low-Earth orbit. The current MW-LST product integrates observations from

six of these satellites. Most important are the Advanced Microwave Scanning Radiometer EOS (AMSR-E) on Aqua from mid-2002 to October 2011 and its successor AMSR2 on the Global Change Observation Mission 1st Water (GCOM-W) from July 2012 onward. Also included are the Special Sensor Microwave and Imager (SSM/I) on platforms F13, F14 and F15 of the Defense Meteorological Satellite Program; the Tropical Rainfall Measurement Mission (TRMM) Microwave Imager (TMI); and Coriolis-WindSat. Together this constellation of Ka-band radiometers allows for the estimation of the diurnal temperature cycle in a process that can be summarized in 4-steps, detailed below and diagrammed in Fig. 1.

2.3.1 Inter-calibration of MW satellites

All available Ka-band observations are combined to create a global record with up to 8 observations per day for each 0.25° resolution grid box. The data are binned in 15–minute windows of local solar time (0:00-0:15 is first window of the day). The brightness temperatures are inter-calibrated using observations from the TRMM satellite (with an equatorial overpass) as a transfer reference. Individual 0.25° averages are masked if the spatial standard deviation of the oversampled Ka-band observations exceeds a prior determined threshold for each grid box. Both the inter-calibration and quality control procedures are described in detail in Holmes et al (2013a). The resulting global record of inter-calibrated Ka-band brightness temperatures spans the years 2003-2013.

2.3.2 Fitting of diurnal cycle model to sparse observations

For days with suitable MW observations (a minimum of 4, at least one of which is close to solar noon) and no $T^{Ka} < 250\ K$ (an indication of frozen soil), a continuous diurnal temperature cycle (DTC) is fitted. The DTC model combines a cosine and an exponential term to describe the effect of the sun and the decrease of surface temperature at night and is based on Göttsche and Olesen (2001) with slight adaptations to limit the number of parameters. This implementation (DTC3) is fully described in Holmes et al. (2015). DTC3 summarizes the DTC with four parameters: daily minimum (T_0) at start and end of day, diurnal amplitude A, and diurnal timing φ. The fitting procedure first determines φ as a temporal constant (Holmes et al., 2013b) and subsequently T_0 and A for each day individually. The success of the fit (ε_d) is expressed as the root mean square error (RMSE) between the modelled and observed T^{Ka} for the n observations (at times t-) in any given day (d), calculated following Eq. (1):

$$\varepsilon_d = \sqrt{\frac{1}{n}\sum_{i=1}^{n}\left(T_i - DTC3(\varphi, T_0, A, t_i)\right)^2} \quad (1)$$

This method was applied to the entire record of inter-calibrated Ka-band brightness temperatures (section 2.3.1) to create a database of annual maps of φ^{Ka}, and daily maps of T_0^{Ka} and A^{Ka}.

2.3.3 Scaling of MW DTC parameters to match TIR-LST target

To relate the diurnal cycle in Ka-band brightness temperature to the composite radiative temperature of the land surface requires a set of DTC parameters that is equivalent to those derived from T^{Ka} but derived from a TIR-LST product. In the present analysis, the TIR-LST that serves as a reference is produced at the Land Surface Analysis, Satellite Application Facility (LSA-SAF). LSA-SAF LST is based on TIR window channels of SEVIRI (Spinning Enhanced Visible and Infra-Red Imager (SEVIRI) on board the Meteosat Second Generation (MSG) geostationary satellite. The same method for fitting a DTC model to sparse observations (section 2.3.2) was applied to the LSA-SAF LST to create a database of annual maps of φ^{TIR} and daily maps of T_0^{TIR} and A^{TIR} (Holmes et al., 2015). This preparation step is diagrammed in Fig 1 as step '0'.

The Ka-band DTC parameters ($T_{0,d}^{Ka}$, A_d^{Ka}) are scaled so that the long-term mean matches that of the equivalent TIR-based parameters ($T_{0,d}^{TIR}$, A_d^{TIR}). Because T_0^{Ka} is affected by the sensing depth, the scaling is performed by using daily mean temperature as an intermediate, which is defined as ($\bar{T}^{Ka} = T_0^{Ka} + A^{Ka}/2$) for this purpose.

$$A_d^{MW} = A_d^{Ka} / \delta \quad (2)$$

$$\bar{T}_d^{MW} = \beta_0 + \beta_1 \bar{T}_d^{Ka} \quad (3)$$

The scaled parameters are indicated with the superscript '*MW*'. The parameter δ represents the slope of the zero-order least squares regression line for estimating the amplitude of A_d^{Ka} from TIR-LST (A_d^{TIR}). The intercept (β_0) and slope (β_1) to correct the mean daily temperature ($\bar{T}_d^{Ka}$) for systematic differences with TIR-LST ($\bar{T}_d^{TIR}$) are determined with a constrained numerical solver, as in Holmes et al. (2015). The constraint is based on radiative transfer considerations and assures that the scaling of the mean is in agreement with the prior scaling of the amplitude (Eq. 2).

The set of time-constant scaling parameters (δ, β_0 and β_1) were determined for each 0.25° grid box based on all days in the period 2007-2012 where both MW and TIR-based DTC parameters were available (generally clear sky and above freezing). Because all three parameters are constant with time, Eqs 2-3 preserve their temporal independence of the TIR LST product. The consequence of using LSA-SAF LST as the reference product is that observation-based scaling parameters are limited to the domain covered by Meteosat (Africa, Europe, Middle-East). Outside this domain, the parameters must be extrapolated. The procedure for the extrapolation is still in development, and currently entails fitting linear regressions with vegetation characteristics. Because of the limited confidence in the scaling parameters outside the MSG-domain, the analysis in this paper is focused on the Africa and Europe domain. Some results of the global set will be presented in the comparison with flux tower observations (Section 3.4).

2.3.4 Constructing MW-LST

Global maps of the time-constant parameters (δ, β_0 and β_1, section 2.3.3) are used to calculate the daily DTC parameters ($T_{0,d}^{MW}, A_d^{MW}$) in the scaled climatology of the TIR-LST product. This scaling (Eqs. 2 and 3) is applied to every day for which estimates of $\bar{T}^{Ka}$ and A^{Ka} are available (see section 2.3.2). The methodology to scale the DTC parameters from this record of Ka-band observations to a physical temperature range is described in more detail in Holmes et al. (2015). The scaled parameters together with φ^{TIR} are then used to construct the MW-LST based on the same DTC3 model as used in step 2:

$$\text{MW-LST}_i = DTC3(\varphi^{TIR}, T_{0,d}^{MW}, A_d^{MW}) \quad (4)$$

The use of the DTC model allows MW-LST to be diurnally complete for days when both $T_{0,d}^{MW}$ and A_d^{MW} are available. MW-LST can therefore be generated at any time increment (i). The MW-LST database used for this paper was generated at 15-minute temporal interval. This allows T_{rad1} and T_{rad2} to be accurately interpolated from the database. ε_d^{Ka} (Eq. 1) is used to flag days where the assumptions imposed by the shape of clear sky DTC3 are not valid or individual Ka-band observations have a large bias. In this experiment, MW-LST was only used if ε_d^{Ka} is 2.5 K or lower.

2.3.54 ~~ALEXI~~ MW-LST in ALEXI~~Model Output~~

~~The output of ALEXI that we focus on in this paper is ET, specifically the 7-day total ET in mm/week (converted from MJ/week by dividing by the heat of vaporization times the density of water, both taken as constants of 2.451 MJ/kg and 1000 kg/m3 respectively).~~ The continuous 7-day totals are achieved by temporal gap-filling of (clear sky) ET as a fraction of clear-sky latent heat flux to incoming solar radiation (Anderson et al., 2007a). To maximize similarity, the same MODIS cloud mask is applied to the ALEXI-MW implementation so that the mechanics of standard ALEXI can be evaluated under circumstances for which it has previously been developed and validated.

The fraction of days in a year where a clear sky MODIS-based T_{rad1} and T_{rad2} is available for ALEXI is below 0.3 for large parts of Europe and (sub)-tropical Africa (Fig 2a). In these areas the revisit time between observation days regularly exceeds 5 days, a threshold for temporal downscaling given the persistence of ET fraction (Alfieri et al., 2017). On average for the non-coast pixels, there is a MW-based estimate available for 69 % of those days where there is also a (clear sky) MODIS-based T_{rad1} and T_{rad2}. The

reason this percentage is not higher is mainly due to the requirement of a near-noon overpass for the fitting of the diurnal temperature curve (See Section 2.3.2), in combination with the 1 in 3 days without such overpass for a given location as determined by the orbit and coverage of Aqua and GCOM-W. This overlap in coverage can support further calibration of MW-LST to MODIS LST, something that is likely needed to maximize consistency between ALEXI implementations over the globe. In terms of potential for additional sampling through the use of MW-based LST, Fig 2c shows that MW-based estimates for the two ALEXI times are available for 54 % of the days where no MODIS-based estimate is available. Fig 2d depicts the fraction of days where either MODIS or MW-LST can be used to estimate the T_{rad} inputs required to run ALEXI. This shows that the addition of MW-LST can bring the minimum average coverage in this domain to once every two days.

2.~~5~~ 4 Flux tower observations

~~Many flux towers include~~Tower measurements of latent heat flux obtained using the eddy-covariance (EC) ~~measurements of ET that~~technique are commonly used for ground truthing of remote sensing and model-based ET estimates (Baldocchi et al., 2001). Harmonized Fluxnet data are distributed in so-called synthesis datasets. They include the original observations at a half hour observation time, and aggregate values per day, week~~ly~~ and month~~ly~~. For this work, we used the synthesis 2015 TIER 1 data as accessed in July 2016 (http://fluxnet.fluxdata.org/data/fluxnet2015-dataset/) to serve as a common ground reference for the evaluation of the temporal characteristics of ALEXI-MW and ALEXI-IR. In particular, the part of the dataset of interest here are the daily aggregates of ~~ET~~ latent heat flux (variable name LE_F_MDS) which include quality control as described in Pastorello et al. (2014).

Based on these daily data, we computed the 7-day averages matching the window length of ALEXI. If not all days within a window have valid data, that window is disregarded. Overall, eddy-covariance observations of ET were available from 68 flux towers with at least one year of observations within the time period of this study.

2.~~6~~ 5 Definition of regions

Although both MW and IR sets are available globally, the main analysis of this paper is focused on the domain encompassing Africa and Europe. This is because only in that region is the scaling of MW-LST to TIR-based LST currently supported by data (see Section 2.3.3). However, ~~purely correlation based~~temporal comparisons (e.g., correlations) are much less affected by the mean absolute value of MW-LST product. Because of the limited availability of ~~Flux~~ flux tower data, we include all available stations from across the globe which allows us to double the amount of stations available for the analysis compared to only the sites in Europe and Africa..

Within the main focus domain of this study we further highlight 11 climate-based domain subsets (see also Fig 3, bottom-right panel):

A. West-African Sahel, Arid
B. West-African Sahel, Semi-Arid
C. Guinean Coast, Dry sub-Humid
D. Central Africa, Humid
E. Horn of Africa, Arid
F. Southern Africa, semi-Arid (large bias in Fig 4)
G. Southern Africa, Arid (large bias in Fig 4)
H. Iberia, semi-Arid
I. Germany, continental Humid
J. European Russia, continental Humid, boreal forest (large bias in Fig 4)
K. France, Humid

These regions are selected to represent a wide variety of seasonal variation in precipitation and climate class, and are based on the work of Trambauer et al. (2014). Rather than attempting to cover the entire domain with these subsets, we selected smaller subsets in order to visualise the local deviations between MW and IR products that might otherwise be averaged out. We also added regions in Europe and several regions that showed a large bias in Fig. 4.

2.~~7~~ 6 Metrics

Cumulative annual and seasonal fluxes are compared in terms of their relative deviation (RD (%)), calculated following Eq. 5:

$$RD = \frac{\bar{x}-\bar{y}}{(\bar{x}+\bar{y})/2} \times 100\% \quad (5)$$

where $\bar{x}$ represents the mean of the MW product and $\bar{y}$ the mean of the IR product, both sampled at the same times. This relative comparison is useful because neither product represents the truth and this formulation places the deviations in context of the size of the fluxes. Still, if the ET is very small (average ET below 14 mm/month) then the denominator becomes too small and the RD is not reported. The temporal agreement between the anomalies in the IR and MW-based ET products is analysed in terms of the Pearson's correlation (ρ), and the spatial agreement in terms of correlation coefficient (R^2).

The temporal agreement of the weekly ET estimates is further compared relative to the flux tower observations that serve as a common reference. For this assessment, MW- and IR-based ET estimates are again compared in terms of ρ but also in terms of root mean square error (RMSE) to quantify the absolute error. The RMSE is calculated following Eq. 7:

$$RMSE = \sqrt{\frac{1}{N}\sum(x-y)^2} \quad (7)$$

where x is the satellite estimate of ET and y is the tower-based measurement of ET. N is the number of data pairs.

3 Results

3.1 Comparing Multi-year means

The mean average ΔT_{rad} as calculated from MW-LST deviates from that calculated from MODIS LST by 0-20 %, which leads to a spatial R^2 of 0.90 (Fig 4. top row). These spatial variations in mean values arise from the different calibration targets. MW-LST is calibrated to match the LSA-SAF LST from MSG (Europe and Africa) with a precision of 2-3K (see Section 2.3.3), and MODIS ΔT_{rad} is trained on GOES (North-America) with an estimated precision of 5-10 % (see Section 2.2). These different calibration domains together with likely calibration differences between GOES and MSG LST products present sources of bias that can explain the regional variation we see in Fig 4. For example, the difference between ΔT_{rad} estimates in the North-East corner of this map may be an artefact of scaling with high incidence angles (θ) for the MSG geostationary satellite. In the farthest corner (θ > 60º), MSG observations were not used and the MW scaling is extrapolated based on land surface characteristics. The MW ΔT_{rad} also exceeds IR-based estimates by more than 10 % in Southern Africa, for which we do not currently have an explanation.

The general agreement in mean ΔT_{rad} translates into a high agreement between IR and MW-based ALEXI in terms of mean annual ET for the period 2003 – 2011. The spatial correlation between MW and IR in terms of ET is 92 % (Fig 4. bottom row), similar to that for ~~,~~ ΔT_{rad} ~~The slightly higher agreement is likely due to physical constraints imposed by the ALEXI retrieval model (e.g. $0<LE<LE_{PT}$).~~. ~~Regions~~ Boreal Russion shows the ~~with~~ most notable differences ~~are Boreal Russia~~in absolute terms, where MW is lower by ~ 20 %. This is related to view angle impacts on the ΔT_{rad} ~~,~~ retrieval, as noted above. MW ET is also much lower than IR ET in the Alps, which likely reflects an interaction between view angle and topography (e.g.., differences in pixel proportion of sunlit and shaded slopes) ~~,~~ ~~and~~In the Horn of Africa, ~~where~~ MW is higher by 20-30%., although little difference in DTRAD is apparent in this region. ALEXI ET becomes more sensitive to small changes in DTRAD near the dry end, where the iterative stress

reduction in transpiration starts to kick in.~~MW ET is also much lower than IR ET in the Alps.~~ ~~Some, but not all of these features are explained by matching opposite bias between IR and MW based Δ.~~

3.2 Regional/Seasonal Bulk Flux comparison

Figure 5 provides a more detailed comparison between the MW and IR products for the domain subsets as described in Section 2.5~~6~~. For each domain subset, it shows the mean monthly total ET and the associated monthly means of ΔT_{rad}. For European Russia (region J) and to a lesser extend Germany (I) and France (K), this shows higher MW-based ΔT_{rad} resulting in lower summertime ET estimates than for ALEXI-IR. Conversely, in the wintertime the lower MW-based ΔT_{rad} results in higher ET estimates compared to the TIR products in October-December. For Iberia (H), the semi-Arid Sahel (B) and Spain (H) there appears to be a difference in timing with MW estimating a later time for peak ET. The higher MW ET estimates in the Horn of Africa are rather uniform over the year, except for December and January where the difference is small. The size of the bias in ET for the Horn of Africa is relatively ~~surprising~~ large compared to the ~~relatively~~ modest bias in ΔT_{rad}. Another disconnect between ΔT_{rad} deviation and ET can be seen in Southern Africa (regions F and G). Despite a general overestimation of ΔT_{rad} by MW the ET estimates are very close to those of ALEXI-IR. The small difference in ET estimates are the opposite of what would be expected from the ΔT_{rad} deviation. Finally, the humid tropical climates of Guinean coast and central Africa (regions C and D) have very little differences in both ΔT_{rad} and ET.

~~For~~ To provide some additional spatial and temporal context ~~to~~ for these observations, the three-month total MW and TIR ET (averaged over 2003-2011) ~~is calculated~~are shown in Fig. 6 for December-January-February (DJF), March-April-May (MAM), June-July-August (JJA) and September-October-November (SON~~), see Fig 6~~). This shows that the cold season overestimation of MW-based ET, seen in the European regions, is present not only in Europe but also in East and Southern Africa in SON. The underestimation of MW-based ET in summer is not as pronounced in terms of its relative difference. The apparent difference in timing, seen in the Sahel and Iberian regions, shows up across the southern border of the Sahara – MW-ET is higher in MAM, and TIR-ET is higher in JJA. The spatial correlation between MW and IR is higher in SON (96 %) and DJF (97 %) compared to the periods MAM (83 %) and JJA (84 %).

D~~d~~espite these localized differences, the transect averages are ~~quite~~remarkably similar showing the general success of scaling MW-LST to TIR-LST (Section 2.3.3).

3.3 Inter-annual Variation

Because the long term mean of MW-LST is calibrated to match a TIR reference (see Section 2.3.3), ~~the~~ a comparison in terms of anomalies is the real test of its performance in the ALEXI framework, especially in areas that are water limited (see Fig. 7). Of the subsets in water-limited regions, the Horn of Africa (ρ=0.78) and Spain (ρ=0.85) subsets show a high degree of correlation between MW and TIR-based ET anomalies. Semi-Arid Southern Africa (F) and the Sahel (B) show relatively poor correlation with ρ=0.48 and ρ=0.63 respectively. The size of the anomaly is much larger for ALEXI-MW in Southern Africa in January and February, reflecting a much larger inter-annual variation.

In energy-limited areas when ET is fully determined based on the meteorological forcing data, the effect of LST inputs is minimal. This is apparent in the Tropical region, where MW and ALEXI-IR have a correlation of 0.99 in Central Africa (region D). Figure 8 shows a map of the correlation between 3-month anomalies of MW and IR-based ALEXI ET.

Seasonal anomalies are calculated by taking the seasonal total ET for a given year and subtracting its corresponding long-term mean seasonal total (2003-2011 period, as shown in Fig 6). Examples of this are shown for a dry year (2008) and a wet year (2011), see Fig 9. Overall the two sets of anomalies agree very well – the MW ALEXI appears to identify roughly the same areas with anomalous high or low ET. The agreement is better in the wet year than in the dry year.

3.4 Comparison with flux tower observations

The availability of eddy-covariance observations of ET from 68 flux towers allows for a more detailed grid-level analysis of temporal agreement. Even at the 0.05-degree (~5 km) resolution of ALEXI-IR there is a large scale miss-match between remote sensing estimate and tower footprint. The impact of this scale difference will depend on the degree of spatial heterogeneity within the larger footprint. We therefore cannot use these flux tower observations to quantify absolute accuracy in either product, but instead focus on its use as a reference target to compare relative performance between two satellite products. To start, we compare the effect of the resolution degradation from 0.05 degree to 0.25 degree. ~~The metrics ρ and RMSE were computed for each flux tower site and listed in Table 2. Overall the mean ρ is very similar for IR and MW ALEXI (ρ=0.76/RMSE=24 Vs ρ=0.74/RMSE=24). At individual stations, the differences may be more pronounced. For ALEXI IR, the majority of the sites have ρ between 0.6 and 0.92, and RMSE of 12-33 mm/week. The metrics for ALEXI MW are very similar on average, see also Fig 10. Surprisingly, at many sites the 0.25° resolution MW product actually outperforms the 0.05° IR product in terms of ρ. Nevertheless, the ρ is generally a bit higher for ALEXI IR, even though the average RMSE comes out the same (24 mm/week).~~

~~Some of the higher values of ρ seen for ALEXI MW might counterintuitively be explained by its coarser resolution.~~ When 0.05° ALEXI-IR is ~~also~~ averaged over its surrounding 0.25° grid (the average of the 5x5 0.05° grid cells) there is an overall improvement in ρ (but ~~and~~ not in RMSE), see Fig 10. Only at three sites does this spatial degradation lower the ρ between the site and the 0.05° grid average higher than with the 0.25° grid box. The landscape heterogeneity is large at these sites (US-Ton, US-Var, and ES-Lgs). For most stations, the spatial degradation actually improves the ρ with the site. In fact, 40 % of the difference in ρ between MW and IR ALEXI is explained by the change in ρ from ALEXI-IR (at 0.05°) to ALEXI-IR (at 0.25°). This indicates the presence of ~~spatially uncorrelated~~ noise in the 0.05° MODIS LST input that is uncorrelated with the surrounding 0.25° grid average and negates any positive effect of its resolution advantage compared to a 0.25° grid average for most sites.

The following analysis compares MW and IR both at 0.25° grid resolution. The metrics we focus on are ρ and RMSE which are computed for each flux tower site and listed in Table 2. For ALEXI-IR, ρ is between 0.6 and 0.92 and RMSE is 12-33 mm/week for the majority of the sites. The impact of LST input varies from site to site (see also Fig 11), with some stations showing higher ρ for ALEXI-MW, but most showing an advantage for ALEXI-IR, as expected. Overall, the mean ρ is higher for ALEXI-IR (ρ=0.78 Vs ρ=0.74), even though the average RMSE comes out the same (24 mm/week).

It is interesting to investigate what drives the difference in temporal correlation at individual sites. The second row in Fig. 1~~0~~ shows how the same data as presented in Fig. 1~~0~~, but broken out based on geographic domain, climate or spatial agreement. The first panel splits the sites by geographic region. Europe and Africa (~~MSG domain,~~ blue) is where MW-LST was calibrated with MSG SEVIRI and the North-American sites (green) is where MODIS ALEXI-IR has been calibrated with GOES data (see Section 2). Between these two groups of stations~~, but~~ the relative improvement in ρ is higher in the North-American sites. ~~(GOES domain, green)~~. This is despite the MODIS ALEXI-IR being calibrated with GOES data. Panel 2 separates the sites based on climate, particularly in terms of the potential ET (PET) relative to the annual precipitation (P). The PET used for this classification is calculated following Priestley-Taylor (1972) with an alpha ~~is~~ parameter of 1.26 and zero ground heat flux. Sites with humid climates (energy limited: PET<=P) have generally a higher ρ between station and satellite data and show only a modest impact of ~~no overall difference in ρ with station data~~the change in LST input on ALEXI. In arid climates (water limited: PET>P) there is more variation in performance and correlations between satellite estimate and tower observation are ~~much~~ generally lower. Partly, this reflects a lower signal to noise in areas with low overall ET, but it also reflects a more challenging environment for ET retrievals. The advantage of ~~and the~~ ALEXI-IR over ALEXI-MW is larger in these arid climates. ~~has an advantage over ALEXI MW.~~ Further subdividing the ~~sites in~~ arid locations based on information on spatial heterogeneity reveals a still larger separation of performance (Fig 1~~0~~, Panel 3 on bottom row). Taking the absolute bias (|b|) between ALEXI-IR at the 0.05° grid cell encompassing the tower site and the mean of the 0.25° surrounding grid box as proxy for spatial heterogeneity, we can see that for the sites that are both in a

water limited region and have a high spatial bias, 11 in total, the average ρ for ALEXI-MW (ρ=0.55) is markedly lower than that for ALEXI-IR (ρ=0.65).

Six of the 68 sites have a markedly higher ρ with ALEXI-IR than with ALEXI-MW. All but one of these sites have an arid climate (See Table 2), and four of those stations also have a high spatial bias between the 0.05° grid box and 0.25° grid box mean (|b|>2 mm/week):

- US-Ton and US-Var (PET/P=2.5/1.7, b=-6.4), Woody Savannas, same 0.05 box. ~~The MODIS~~ALEXI-IR has a ρ=0.80/0.5, while ~~the~~ ALEXI-MW has a ~~poor~~ lower value of 0.56/0.09. ~~Especially~~ At US-Var, the site has an abrupt collapse of ET at end of summer ~~that~~. The satellite data miss~~es~~ this, especially the ALEXI-MW(0.25°) product.
- Zambia, Savannas. ZM-Mon. Water limited (PET/P=2.3), spatial heterogeneous (b=-2.9)
- ES-LgS, Woody Savannas (b=11, PET/P=2.8). The MODIS has a high ρ=0.84, while the MW has a poor ρ=0.62. The average comes in at ρ=0.82. This site is located on a mountain ridge. The smaller grid size of ALEXI-IR is able to capture the vegetation conditions at the mountain ridges whereas the 0.25 grid of ALEXI-MW has more bare soil which leads to lower ET values.

The station in Sudan (SD-Dem) is the only of these 6 stations that is in a water limited region (arid desert climate) and has low spatial bias. Despite the low bias, the station ET estimates are 2.5 times satellite estimates, so it could be that the near station land use is not representative of the wider area.

The final station that shows a large advantage in ρ for ALEXI-IR relative to ALEXI-MW is Fi-Hyy (No. 63 in Table 2) in a cold region climate. It is also one of only two stations with data availability at high latitude (above 60°N). This station has land cover dominated by evergreen needleleaf forest. The bias between the 0.05° and 0.25° grid box mean is also small (b=-0.6). The MW observations have relatively many weeks with very low ET estimates compared to the ALEXI-IR. The reason for this is not readily apparent but it could be that the MW product suffers from rainclouds that suppress temperature estimates during the morning hours around ALEXI time 1. This, in turn, leads to an overestimated morning temperature rise.

In contrast to these sites, there are two sites where the ALEXI-MW outperforms ALEXI-IR in terms of correlation with in situ sites despite being in a relatively arid climate with large spatial bias: US-SRG, US-NR1. For US-NR1, ρ is low because station records high values in winter time, and the site is located in an evergreen forest east of a mountain ridge, with high day to day variation, possibly due to varying wind direction or shading effects. Despite this, both satellite products pick up the seasonal cycle reasonably well, except that they both underestimate wintertime ET.

~~3.5 Prospects for merging MW- and TIR-based ALEXI~~

~~The above analysis of flux tower data suggests that the prospect for merging MW and TIR is good for humid climate regions and also for more arid regions but with the additional condition of requiring a more spatially homogeneous landscape at the 0.25° grid scale. In arid climates, the overall correlation between satellite retrievals and tower sites is relative poor. This is expected because the signal to noise is reduced in areas with low seasonal variation in ET. The change in input LST from IR to MW reduces the ρ on average by 0.04 in the arid climates. Even so, it seems that only if there is also local heterogeneity at the 0.25° grid resolution will the prospect for merging ALEXI MW and ALEXI IR require more complex procedures to avoid degradation relative to the ALEXI IR generate at 0.05° grid resolution.~~

~~In fact, as a simple test of a potential merging of MW and IR based ALEXI ET estimates we calculated the simple average of MW (at 0.25° resolution) and TIR based (at 0.05° resolution) 7 day ALEXI ET totals (ALEXI IR+MW) and re calculated the correlation and RMSE with the flux tower sites. Fig 12 shows a visual comparison of these temporal metrics with the tower observations, analogous to Fig. 10 but now with the results for ALEXI IR+MW on the y axis instead of ALEXI MW independently. In the top, left hand panel, most stations now appear below the 1:1 line, showing a general increase in ρ as a result of simply averaging ALEXI IR and ALEXI MW. Indeed, by averaging the weekly ET estimates the ρ is improved from an average of 0.76 for ALEXI IR to 0.78~~

~~for ALEXI IR+MW. The change in correlation is significant for 12 of the 68 stations (according to a Fischer z test), and those stations improve from an average of 0.69 for ALEXI IR to 0.75 for ALEXI IR+MW (see also Table 2). The top right-hand panel shows a comparison of RMSE values calculated between ALEXI IR and the station data, and between ALEXI IR+MW and the station data. Values above the line indicate a reduction in RMSE for the combined product compared to ALEXI IR product. The individual station results are all close to the 1:1 line, and the mean RMSE reduces from 24 mm/week to 23 mm/week. The bottom row of the figure shows results broken down by subsets of stations based on domain, climate or spatial bias as was done for Fig 10, above. This shows when taking the simple average of ALEXI IR and ALEXI MW, the overall correlation improves for all but the most challenging conditions. Even for the subset where the relative performance for ALEXI MW was poorest (stations water limited climate and with a spatial bias between the 0.05° and 0.25° grid box), the correlation is very close to that of the ALEXI IR alone (ρ=0.64 vs. ρ=0.65).~~

4 Discussion and Conclusion

This paper shows that a newly developed MW-LST product can be used to effectively substitute TIR-based LST in a two-source energy balance approach to estimate coarse-resolution ET (~25 km) from space. This particular TSEB approach, the ALEXI model framework, is an approach that minimizes sensitivity to absolute biases in input records of LST through the analysis of the rate of change in morning LST. It is therefore an important test of the ability to retrieve diurnal temperature information from a constellation of satellites that provide 6-8 observations of Ka-band brightness temperature per location per day. This represents the first ever attempt at a global implementation of ALEXI with MW-based LST and is intended as the first step towards providing all-weather capability to the ALEXI framework.

Because the long-term (7-year mean) diurnal features of MW-LST are calibrated to TIR-LST, it is perhaps not surprising that the long-term bulk ET estimates agree with a spatial correlation of 92 % for total ET in the Europe/Africa domain. A comparison with biases in the input datasets of ΔT_{rad} shows that a large part of the remaining differences can be mitigated by specifically calibrating MW-LST to MODIS LST. More convincing is the agreement in seasonal (3-month) averages of and 83-97 % because the calibration is based on time-constant parameters. Adding another layer of challenging complexity is the comparison in terms of 3-month anomalies. By this test, ALEXI-MW also matches ALEXI-IR very closely, demonstrating an ability to capture the development and extent of drought conditions.

The two parallel ALEXI implementations are further compared at the maximum temporal resolution of the current global ALEXI output (7 days) and relative to a common ground measured reference provided by the FLUXNET consortium. The 68 stations that were available for this analysis represent a wide range of land cover characteristics and climate conditions. Overall, they indicate a ~~surprisingly~~ close match in both performance metrics (ρ and RMSE), especially considering the advantage of TIR-LST compared to MW-LST in these clear sky conditions. The ~~for all but the~~ most challenging ~~sites~~ conditions for MW-LST as input to ALEXI-ET according to these sites are locations with higher aridity levels and where the larger domain has a high ~~in terms of~~ spatial heterogeneity ~~and level aridity~~. Spatial heterogeneity places an obvious penalty on ALEXI-MW due to the coarser MW-LST input, even though in general ALEXI-IR improves in terms of its correlation with the tower data when it is spatially downgraded to 0.25° resolution. ~~In terms of climate, the sensitivity of ALEXI ET retrievals to the LST input increases with increasing water limitation of evapotranspiration. In humid climates, the ET estimate is close to the potential ET, which is calculated based on meteorological forcing.~~ For future merging of IR- and MW-based ALEXI into a superior combined ET estimate this range in relative performance observed at these sites needs to be accounted for.

~~As an experiment, we also calculated the average of ALEXI IR and ALEXI MW, both at their original spatial resolutions (0.05° and 0.25° respectively) and calculated the same temporal performance metrics with the station observations. Since they are derived from~~

~~completely difference remote sensing techniques, errors in the temporal features of MW-LST should be independent of those in TIR-LST. Moreover, because LST is one of the main diagnostic inputs to ALEXI the LST related errors in retrieved ET are also expected to be independent. This, in turn, is expected to allow for a reduced estimation uncertainty of ET by averaging two independent estimates of the same variable. The overall observed improvement from ρ=0.76 to ρ=0.78 confirms this expectation that part of the error in ET estimates from ALEXI-IR and ALEXI-MW is independent.~~

Based on the analyses presented in this paper, we outline the following roadmap for an all-sky implementation of ALEXI-MW. First of all, there is a need for global observation based calibration of MW-LST with MODIS-LST to reduce biases as identified at the high incidence angles of the MSG domain and avoid the need for extrapolation of scaling parameters. Second, the MW-LST could be used to improve the TIR cloud mask by attributing anomalous TIR-based ΔT_{rad} to the presence of clouds, with subsequent improvements in ALEXI-IR ET estimates. ~~Finally, it appears that a simple averaging of ALEXI-IR and ALEXI-MW would provide for a reduction in estimation uncertainty of ALEXI ET for times when both are available.~~ Finally, the all-sky implementation that is now within reach with ALEXI-MW will test the assumptions in new ways, which will require careful investigation. For example, the assumptions related to the boundary layer development may be tested as we move to include less stable conditions associated with cloudy skies. Similarly, evaporation of intercepted rain water will feature more prominently under cloudy skies and may require inclusion as a separate process within the current physical framework. With a combined MW+IR ALEXI estimates it appears entirely feasible to reduce the current window length for reporting MODIS ALEXI ET totals from 7-days to as low as 2. At a window length of 2 days the average satellite coverage would support each 2-day total with at least one ~~observation~~ET retrieval (See Fig. 2). This would reduce the reliance on temporal downscaling and its associated assumptions and impact on estimation error. More independent estimates of ET would allow for more robust statistical analysis in the context of land-atmosphere exchange studies, even if the record length is not extended. Perhaps most importantly, a shorter reporting interval would also allow for earlier detection of agricultural drought as reflected in the ET-based drought indices (Anderson et al., 2011).

Data Availability

The ALEXI-IR data is available from NASA SPoRT (MSFC). The ALEXI-MW is an intermediate research product available upon request. Time-series of ALEXI-MW and ALEXI-IR covering the site locations and time period of this paper are available upon request from the corresponding author. The Flux tower data is publicly available through the FLUXNET community as detailed in Section 2.3~~4~~.

Acknowledgements

We thank the reviewers for their insightful comments on this manuscript. This work was funded by NASA through the research grant “The Science of Terra and Aqua” (13-TERAQ13-0181).

References

Alfieri, J. G., Anderson, M. C., Kustas, W. P. and Cammalleri, C.: Effect of the revisit interval and temporal upscaling methods on the accuracy of remotely sensed evapotranspiration estimates, Hydrol. Earth Syst. Sci., 21(1), 83–98, doi:10.5194/hess-21-83-2017, 2017.

Anderson, M. C., Norman, J. M., Diak, G. R., Kustas, W. P. and Mecikalski, J. R.: A two-source time-integrated model for estimating surface fluxes using thermal infrared remote sensing, Remote Sens. Environ., 60(2), 195–216, 1997.

Anderson, M. C., Norman, J. M., Mecikalski, J. R., Otkin, J. A. and Kustas, W. P.: A climatological study of evapotranspiration and moisture stress across the continental United States based on thermal remote sensing: 1. Model formulation, J. Geophys. Res., 112(D10), D10117, 2007a.

Anderson, M. C., Norman, J. M., Mecikalski, J. R., Otkin, J. A. and Kustas, W. P.: A climatological study of evapotranspiration and moisture stress across the continental United States based on thermal remote sensing: 2. Surface moisture climatology, J. Geophys. Res. Atmospheres, 112(D11), doi:doi:10.1029/2006JD007507, 2007b.

Anderson, M. C., Kustas, W. P., Norman, J. M., Hain, C. R., Mecikalski, J. R., Schultz, L., Gonzalez-Dugo, M. P., Cammalleri, C., d'Urso, G. and Pimstein, A.: Mapping daily evapotranspiration at field to continental scales using geostationary and polar orbiting satellite imagery, Hydrol. Earth Syst. Sci., 15(1), 223, 2011.

Baldocchi, D., Falge, E., Gu, L. H., Olson, R., Hollinger, D., Running, S., Anthoni, P., Bernhofer, C., Davis, K., Evans, R., Fuentes, J., Goldstein, A., Katul, G., Law, B., Lee, X. H., Malhi, Y., Meyers, T., Munger, W., Oechel, W., U, K., Pilegaard, K., Schmid, H. P., Valentini, R., Verma, S., Vesala, T., Wilson, K. and Wofsy, S.: FLUXNET: A new tool to study the temporal and spatial variability of ecosystem-scale carbon dioxide, water vapor, and energy flux densities., Bull Am Meteorol Soc, 82, 2415–2434, 2001.

Campbell, G. S. and Norman, J. M.: An Introduction to environmental biophysics, Springer-Verlag, New York [etc., 1998.

Doelling, D.: CERES Level 3 SYN1DEG-DAYTerra+Aqua netCDF file - Edition 3A, , doi:10.5067/Terra+Aqua/CERES/SYN1degDAY_L3.003A, 2012.

Friedl, M. A., Sulla-Menashe, D., Tan, B., Schneider, A., Ramankutty, N., Sibley, A. and Huang, X.: MODIS Collection 5 global land cover: Algorithm refinements and characterization of new datasets, Remote Sens. Environ., 114(1), 168–182, 2010.

Göttsche, F.-M. and Olesen, F. S.: Modelling of diurnal cycles of brightness temperature extracted from METEOSAT data, Remote Sens. Environ., 76(3), 337–348, doi:10.1016/S0034-4257(00)00214-5, 2001.

Hain, C. R. and Anderson, M. C.: Estimating Morning Change in Land Surface Temperature from MODIS Day/Night Land Surface Temperature: Applications for Surface Energy Balance Modeling, in press.

Hain, C. R., Crow, W. T., Anderson, M. C. and Yilmaz, M. T.: Diagnosing Neglected Soil Moisture Source–Sink Processes via a Thermal Infrared–Based Two-Source Energy Balance Model, J. Hydrometeorol., 16(3), 1070–1086, doi:10.1175/JHM-D-14-0017.1, 2015.

Holmes, T. R. H., Crow, W. T., Yilmaz, M. T., Jackson, T. J. and Basara, J. B.: Enhancing model-based land surface temperature estimates using multiplatform microwave observations, J. Geophys. Res. Atmospheres, 118, 577–591, doi:10.1002/jgrd.50113, 2013a.

Holmes, T. R. H., Crow, W. T. and Hain, C.: Spatial patterns in timing of the diurnal temperature cycle, Hydrol. Earth Syst. Sci., 17(10), 3695–3706, doi:10.5194/hess-17-3695-2013, 2013b.

Holmes, T. R. H., Crow, W. T., Hain, C. R., Anderson, M. and Kustas, W. P.: Diurnal temperature cycle as observed by thermal infrared and microwave radiometers., Remote Sens. Environ., 158C, 110–125, doi:10.1016/j.rse.2014.10.031, 2015.

Holmes, T. R. H., Hain, C. R., Anderson, M. C. and Crow, W. T.: Cloud tolerance of remote-sensing technologies to measure land surface temperature, Hydrol. Earth Syst. Sci., 20(8), 3263–3275, doi:10.5194/hess-20-3263-2016, 2016.

Kustas, W. P. and Norman, J. M.: Evaluation of soil and vegetation heat flux predictions using a simple two-source model with radiometric temperatures for partial canopy cover, Agric. For. Meteorol., 94(1), 13–29, 1999.

Mecikalski, J. R., Diak, G. R., Anderson, M. C. and Norman, J. M.: Estimating fluxes on continental scales using remotely sensed data in an atmospheric-land exchange model, J. Appl. Meteorol., 38(9), 1352–1369, 1999.

Myneni, R. B., Hoffman, S., Knyazikhin, Y., Privette, J. L., Glassy, J., Tian, Y., Wang, Y., Song, X., Zhang, Y., Smith, G. R. and others: Global products of vegetation leaf area and fraction absorbed PAR from year one of MODIS data, Remote Sens. Environ., 83(1), 214–231, 2002.

Norman, J. M., Kustas, W. P. and Humes, K. S.: Source approach for estimating soil and vegetation energy fluxes in observations of directional radiometric surface temperature, Agric. For. Meteorol., 77(3–4), 263–293, doi:10.1016/0168-1923(95)02265-Y, 1995.

Norouzi, H., Rossow, W., Temimi, M., Prigent, C., Azarderakhsh, M., Boukabara, S. and Khanbilvardi, R.: Using microwave brightness temperature diurnal cycle to improve emissivity retrievals over land, Remote Sens. Environ., 123, 470–482, 2012.

Pastorello, G., Agarwal, D., Papale, D., Samak, T., Trotta, C., Ribeca, A., Poindexter, C., Faybishenko, B., Gunter, D., Hollowgrass, R. and others: Observational data patterns for time series data quality assessment, in 2014 IEEE 10th International Conference on e-Science, vol. 1, pp. 271–278, IEEE, Sao Paulo, Brazil., 2014.

Priestley, C. H. B. and Taylor, R. J.: On the assessment of surface heat flux and evaporation using large-scale parameters, Mon. Weather Rev., 100(2), 81–92, 1972.

Prigent, C., Jimenez, C. and Aires, F.: Towards "all weather", long record, and real-time land surface temperature retrievals from microwave satellite observations, J. Geophys. Res. Atmospheres [online] Available from: http://onlinelibrary.wiley.com/doi/10.1002/2015JD024402/full (Accessed 17 May 2016), 2016.

Rossow, W. B., Garder, L. C. and Lacis, A. A.: Global, Seasonal Cloud Variations from Satellite Radiance Measurements. Part I: Sensitivity of Analysis, J. Clim., 2(5), 419–458, doi:http://dx.doi.org/10.1175/1520-0442(1989)002<0419:GSCVFS>2.0.CO;2, 1989.

Saha, S. and al: NCEP Climate Forecast System Version 2 (CFSv2) 6-hourly Products, [online] Available from: http://dx.doi.org/10.5065/D61C1TXF, 2011.

Saha, S. and et al: NCEP Climate Forecast System Reanalysis (CFSR) 6-hourly Products, January 1979 to December 2010., [online] Available from: http://dx.doi.org/10.5065/D69K487J, 2010.

Schaaf, C. B., Gao, F., Strahler, A. H., Lucht, W., Li, X., Tsang, T., Strugnell, N. C., Zhang, X., Jin, Y., Muller, J.-P., Lewis, P., Barnsley, M., Hobson, P., Disney, M., Roberts, G., Dunderdale, M., Doll, C., d'Entremont, R. P., Hu, B., Liang, S., Privette, J. L. and Roy, D.: First operational BRDF, albedo nadir reflectance products from MODIS, Remote Sens. Environ., 83(1–2), 135–148, doi:10.1016/S0034-4257(02)00091-3, 2002.

Trambauer, P., Dutra, E., Maskey, S., Werner, M., Pappenberger, F., Van Beek, L. P. H. and Uhlenbrook, S.: Comparison of different evaporation estimates over the African continent, Hydrol. Earth Syst. Sci., 18(1), 193, doi:doi:10.5194/hess-18-193-2014, 2014.

Trenberth, K. E., Fasullo, J. T. and Kiehl, J.: Earth's global energy budget, Bull. Am. Meteorol. Soc., 90(3), 311, 2009.

Ulaby, F. T., Moore, R. K. and Fung, A. K.: Microwave Remote Sensing: Active and Passive. Vol. III. From theory to applications., Artech House, Norwood, MA., 1986.

Wan, Z.: New refinements and validation of the MODIS land-surface temperature/emissivity products, Remote Sens. Environ., 112(1), 59–74, doi:10.1016/j.rse.2006.06.026, 2008.

Table 1. Primary inputs for current global implementation of ALEXI

Data	Purpose	Source	Spatial Resolution
LST	T_{rad}, Net Radiation	MODIS (MYD11C1) (Section 2.2)	0.05°
		MW-LST (Section 2.1)	0.25°
Surface Longwave Radiation	Net Radiation	CFS-R[2], CFSRv2[3]	0.5°
Surface Shortwave Fluxes	Net Radiation	CERES SYN1deg[4]	1°
Albedo	Net Radiation	MODIS (M~~O~~CD43B3~~C~~)[5]	0.05°
LAI	Trad partitioning	MODIS (~~MOD15A~~MCD15A3)[6]	0.01°
Landcover type	Canopy characteristics	~~UMD~~[7]MODIS (MCD12C1)[7]	0.01°
Wind speed	Aerodynamic resistance	CFS-R, CFSRv2	0.5°
Lapse rate profile	Atmospheric Boundary layer growth model	CFS-R, CFSRv2	0.5°

[2]NCEP Climate Forecast System Reanalysis (Saha and et al, 2010), [3] (Saha and al, 2011), [4] (Doelling, 2012), [5](Schaaf et al., 2002), [6](Myneni et al., 2002), [7](Friedl et al., 2010)

Table 2. Time-series correlation of flux tower ET observations with three alternative satellite-based ET estimates (ALEXI_IR, ALEXI-MW, ALEXI- IR+MW). Comparison is based on weekly averages in the period of 2003 to 2011 (number of data pairs is noted in the table). Bias is mean difference between 0.05 grid and 0.25 surrounding grid average as measured by ALEXI-IR.

No.	Site ID	Latitude	Longitude	IGBP Vegetation Type	Climate PET/P	bias	Data pairs (wk)	ALEXI-IR (0.05) ~~ρR~~	ALEXI-IR (0.05) RMSE	ALEXI-MW (0.25) ~~ρR~~	ALEXI-MW (0.25) RMSE	ALEXI-IR+MW (Avg) ~~ρR~~	ALEXI-IR+MW (Avg) RMSE
1	AT-Neu	47.11667	11.3175	Mix. Forests	0.67	-1.26	380	0.78	22.8	0.90	17.7	0.83	23.7
2	AU-Ade	-13.0769	131.1178	Savannas	N/A	-1.12	77	0.87	51.0	0.87	49.9	0.84	43.3
3	AU-DaP	-14.0633	131.3181	Savannas	0.94	-0.85	190	0.82	37.7	0.83	38.2	0.70	37.0
4	AU-DaS	-14.1593	131.388	Savannas	0.85	3.09	178	0.77	32.3	0.79	34.5	0.70	25.6
5	AU-Dry	-15.2588	132.3706	Savannas	6.63	4.41	107	0.56	32.2	0.58	35.3	0.48	26.6
6	AU-Stp	-17.1508	133.3503	Grasslands	1.54	-1.02	142	0.59	40.1	0.59	39.6	0.72	32.0
7	AU-Tum	-35.6566	148.1516	ENF	0.96	2.52	289	0.85	22.6	0.83	25.3	0.79	24.6
8	AU-Wac	-37.429	145.1873	EBF	0.13	8.53	132	0.80	20.1	0.80	24.2	0.80	20.6
9	AU-Wom	-37.4222	144.0944	EBF	0.78	0.65	77	0.84	29.1	0.86	29.2	0.82	25.2
10	BE-Bra	51.30917	4.520556	Mix. Forests	0.57	-0.74	308	0.81	14.0	0.83	12.5	0.73	14.1
11	BE-Lon	50.55219	4.744772	Croplands	0.61	0.09	309	0.84	15.4	0.85	15.2	0.86	15.3
12	BE-Vie	50.30507	5.998052	Mix. Forests	0.61	0.47	274	0.85	13.2	0.84	13.6	0.74	16.2
13	CA-Qfo	49.69247	-74.342	ENF	0.56	-0.32	308	0.69	14.8	0.76	13.0	0.82	11.6
14	CA-SF1	54.48495	-105.817	ENF	0.93	0.52	130	0.78	24.6	0.80	23.9	0.70	32.8
15	CA-SF2	54.25392	-105.878	Mix. Forests	1.82	0.77	114	0.70	25.5	0.75	24.2	0.59	32.0
16	CA-SF3	54.09156	-106.005	ENF	0.91	2.21	155	0.81	16.0	0.82	15.4	0.80	17.5
17	CH-Cha	47.21022	8.410444	Mosaic	0.46	-5.44	257	0.87	38.8	0.93	32.2	0.89	29.3
18	CH-Dav	46.81533	9.855917	ENF	0.75	-0.14	413	0.54	26.5	0.61	24.3	0.59	29.9
19	CH-Fru	47.11583	8.537778	Mosaic	0.39	3.77	241	0.90	21.6	0.89	25.3	0.80	28.6
20	CN-Du2	42.04667	116.2836	Grasslands	1.99	1.10	101	0.62	24.8	0.65	25.1	0.68	24.8
21	CZ-wet	49.02465	14.77035	Croplands	0.94	1.65	101	0.92	13.0	0.92	13.8	0.88	15.8
22	DE-Geb	51.1001	10.9143	Croplands	0.81	-1.18	411	0.85	15.5	0.86	14.8	0.77	19.4
23	DE-Gri	50.94947	13.51253	Mixed Forests	0.52	-0.38	329	0.88	12.2	0.89	11.6	0.88	12.3
24	DE-Hai	51.07917	10.453	Mix. Forests	0.68	3.15	322	0.91	13.0	0.92	13.7	0.87	19.8
25	DE-Kli	50.89288	13.52251	Croplands	0.46	-1.26	284	0.84	14.3	0.87	14.0	0.84	15.4
26	DE-Lkb	49.09962	13.30467	ENF	0.45	1.38	92	0.84	14.6	0.84	14.8	0.79	15.0
27	DE-Obe	50.78362	13.71963	ENF	0.53	3.09	167	0.87	13.4	0.86	13.3	0.83	14.0
28	DE-Seh	50.87062	6.449653	Croplands	0.63	0.48	132	0.84	24.1	0.85	24.0	0.80	29.3
29	DE-Tha	50.96361	13.56694	ENF	0.65	1.63	413	0.86	14.0	0.88	12.1	0.88	11.8
30	ES-LgS	37.09794	-2.96583	Woody Savannas	2.01	11.28	92	0.84	11.3	0.77	17.1	0.62	18.3
31	FI-Hyy	61.8475	24.295	ENF	0.84	-0.61	312	0.84	13.4	0.85	12.8	0.65	22.5
32	FI-Sod	67.36186	26.63783	ENF	0.49	-0.08	185	0.47	22.5	0.46	22.2	0.43	25.9
33	FR-Gri	48.84422	1.95191	Croplands	0.75	-1.18	232	0.82	21.6	0.83	20.5	0.81	19.8
34	IT-Col	41.84936	13.58814	DBF	0.88	-0.67	180	0.72	20.4	0.74	18.6	0.79	18.1
35	IT-Lav	45.9562	11.28132	ENF	0.65	0.99	395	0.81	18.8	0.81	20.0	0.78	22.6
36	IT-MBo	46.01468	11.04583	Grasslands	0.52	3.15	419	0.82	20.9	0.84	21.4	0.87	17.6
37	IT-PT1	45.20087	9.061039	Croplands	1.09	1.63	78	0.94	16.8	0.92	19.3	0.92	19.3
38	IT-Ren	46.58686	11.43369	ENF	0.62	0.53	360	0.75	33.0	0.80	32.6	0.77	34.5
39	IT-Tor	45.84444	7.578055	ENF	0.72	-2.27	122	0.62	31.8	0.72	29.1	0.61	40.2
40	NL-Loo	52.16658	5.743556	ENF	0.83	-0.70	380	0.70	28.9	0.70	28.4	0.67	26.1
41	RU-Fyo	56.46153	32.92208	Mixed Forests	0.80	0.82	314	0.83	17.5	0.84	17.1	0.71	25.2
42	SD-Dem	13.2829	30.4783	Grasslands	3.13	1.19	112	0.76	41.9	0.80	43.2	0.47	43.0
43	US-AR1	36.4267	-99.42	Grasslands	1.42	3.06	131	0.75	31.0	0.76	33.4	0.78	24.9
44	US-AR2	36.6358	-99.5975	Grasslands	1.48	0.38	121	0.75	20.2	0.77	19.9	0.76	15.7
45	US-ARM	36.6058	-97.4888	Croplands	1.21	-3.34	409	0.72	21.7	0.72	20.1	0.69	19.3
46	US-ARb	35.54974	-98.0402	Croplands	1.28	1.87	78	0.82	31.0	0.82	32.2	0.89	28.3
47	US-ARc	35.54649	-98.0401	Grasslands	1.27	1.87	84	0.86	37.5	0.85	39.5	0.89	35.1
48	US-Blo	38.89525	-120.633	ENF	0.82	0.81	206	0.82	27.9	0.84	27.3	0.89	21.5
49	US-Cop	38.09	-109.39	Grasslands	4.33	-2.16	87	0.22	11.8	0.31	9.7	0.33	9.8
50	US-GLE	41.3644	-106.239	ENF	0.41	10.44	261	0.46	27.2	0.46	27.5	0.37	36.1
51	US-Los	46.08268	-89.9792	Mixed Forests	0.71	0.06	271	0.75	19.3	0.85	20.2	0.86	23.7
52	US-MMS	39.32315	-86.4131	DBF	0.68	3.91	439	0.91	15.9	0.90	17.8	0.88	18.6
53	US-Me2	44.4523	-121.557	ENF	2.07	0.35	374	0.73	30.9	0.75	31.2	0.72	28.4
54	US-NR1	40.03288	-105.546	ENF	1.11	-4.20	449	0.64	21.0	0.70	18.2	0.73	25.0
55	US-Ne1	41.16506	-96.4766	Croplands	0.89	-0.86	427	0.88	34.0	0.89	32.9	0.87	31.7
56	US-Ne2	41.16487	-96.4701	Croplands	0.87	-0.86	434	0.87	32.1	0.87	31.2	0.85	30.4
57	US-Ne3	41.17967	-96.4396	Croplands	1.00	-0.42	420	0.88	27.4	0.89	26.6	0.87	25.8
58	US-SRG	31.7894	-110.828	Grasslands	N/A	6.65	178	0.67	28.2	0.66	33.7	0.74	25.3
59	US-SRM	31.82143	-110.866	Open Shrublands	2.78	-1.89	397	0.50	28.3	0.58	26.6	0.67	19.6
60	US-Syv	46.24202	-89.3477	Mix. Forests	0.87	0.57	171	0.88	17.8	0.89	15.2	0.91	15.6
61	US-Ton	38.4316	-120.966	Woody Savannas	1.86	-6.37	353	0.80	16.1	0.75	15.4	0.56	22.8
62	US-Twt	38.1055	-121.652	Croplands	1.68	1.89	108	0.78	73.1	0.81	72.2	0.72	74.1
63	US-Var	38.40667	-120.951	Woody Savannas	1.28	-6.37	428	0.50	21.1	0.35	24.2	0.09	34.2
64	US-WCr	45.80593	-90.0799	DBF	0.82	0.04	194	0.78	20.5	0.84	18.3	0.82	19.3
65	US-Whs	31.74383	-110.052	Open Shrublands	3.32	4.02	228	0.69	17.4	0.76	19.1	0.64	20.0
66	US-Wkg	31.73653	-109.942	Grasslands	2.78	0.67	389	0.61	19.0	0.68	19.3	0.73	15.5
67	ZA-Kru	-25.0197	31.4969	Savannas	2.85	-2.33	180	0.62	30.3	0.64	29.6	0.57	31.1
68	ZM-Mon	-15.4378	23.25278	Savannas	1.68	-2.88	92	0.76	24.8	0.78	22.9	0.53	26.8

ENF: Evergreen Needleleaf Forest, DBF: Deciduous Broadleaf Forest, EBF: Evergreen Broadleaf Forest, Mosaic: Cropland/Natural Vegetation Mosaic

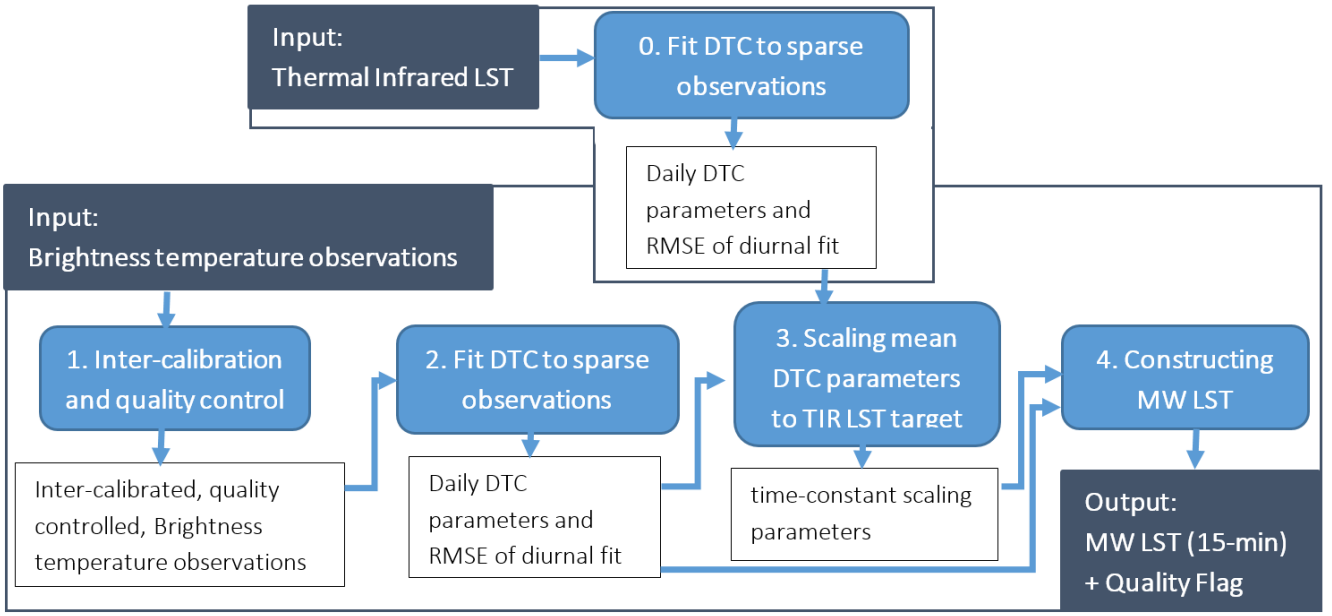

Figure 1: MW-LST workflow

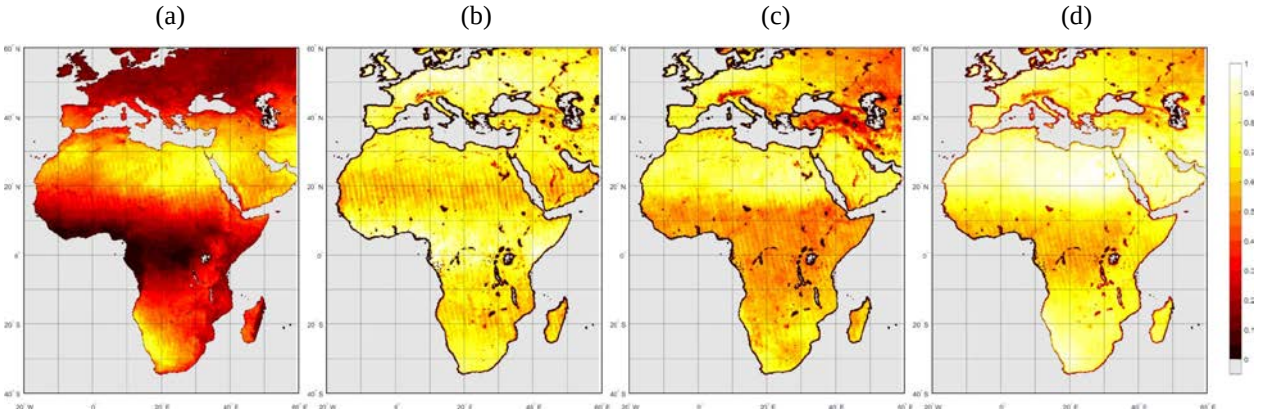

Figure 2: Temporal coverage of MW and IR-based ΔT_{rad} in 2004. Panel a shows the fraction of total days where MODIS-based estimates of ΔT_{rad} are available. Panel b shows the fraction of this subset of days where there is also a MW-based ΔT_{rad} available. Panel c shows the fraction of days without a MODIS-based estimate but with availability of a MW-based estimate (potential for IR-gap coverage). Panel d shows the fraction of total days where either a MODIS- or a MW-based ΔT_{rad} is available.

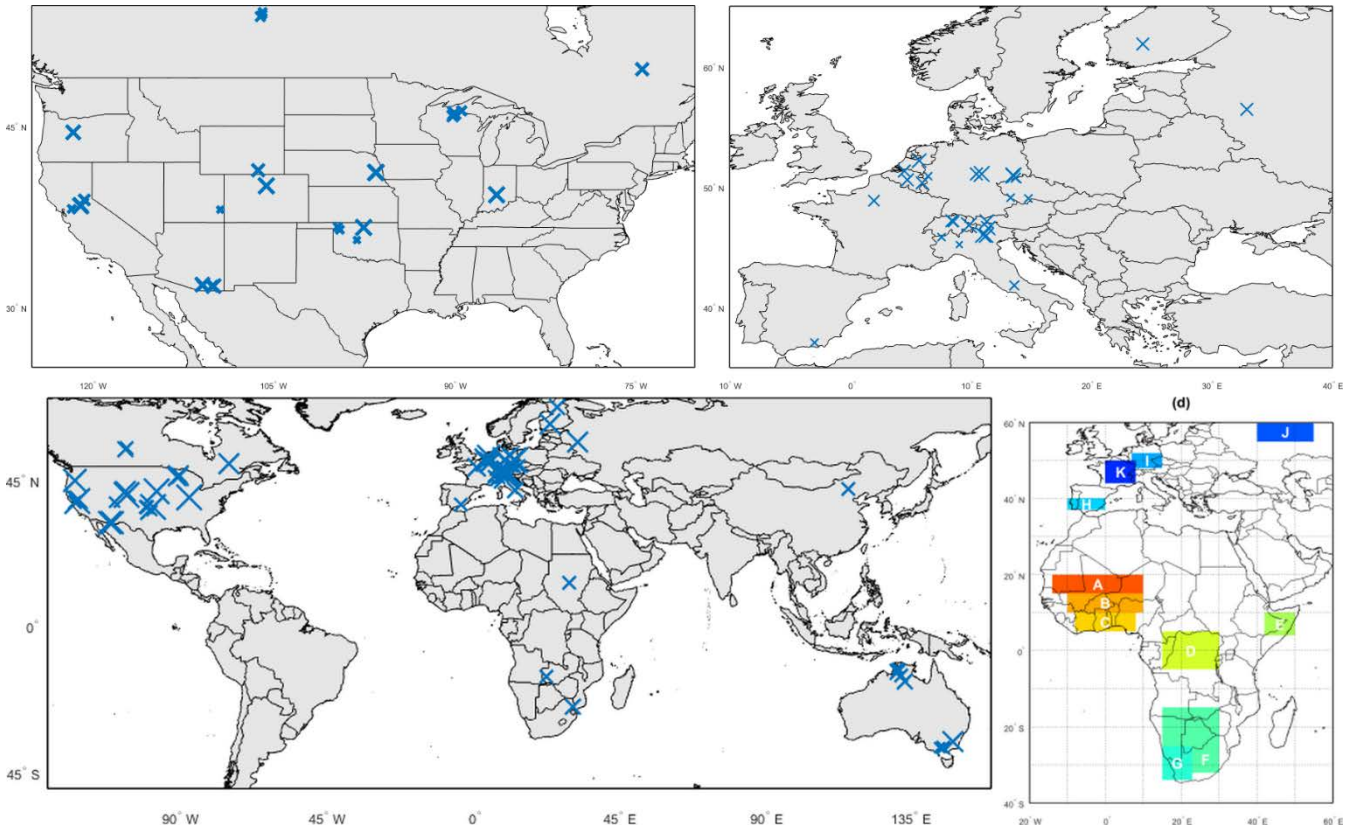

Figure 3: Location of flux tower sites used in the analysis (see also Table 2): (a) North America, (b) Europe, (c) World. The size of the marker is in proportion to number of data days used in assessment. Panel (d) indicates the ~~12~~ 11 regions selected based on annual precipitation cycle and geographic diversity.

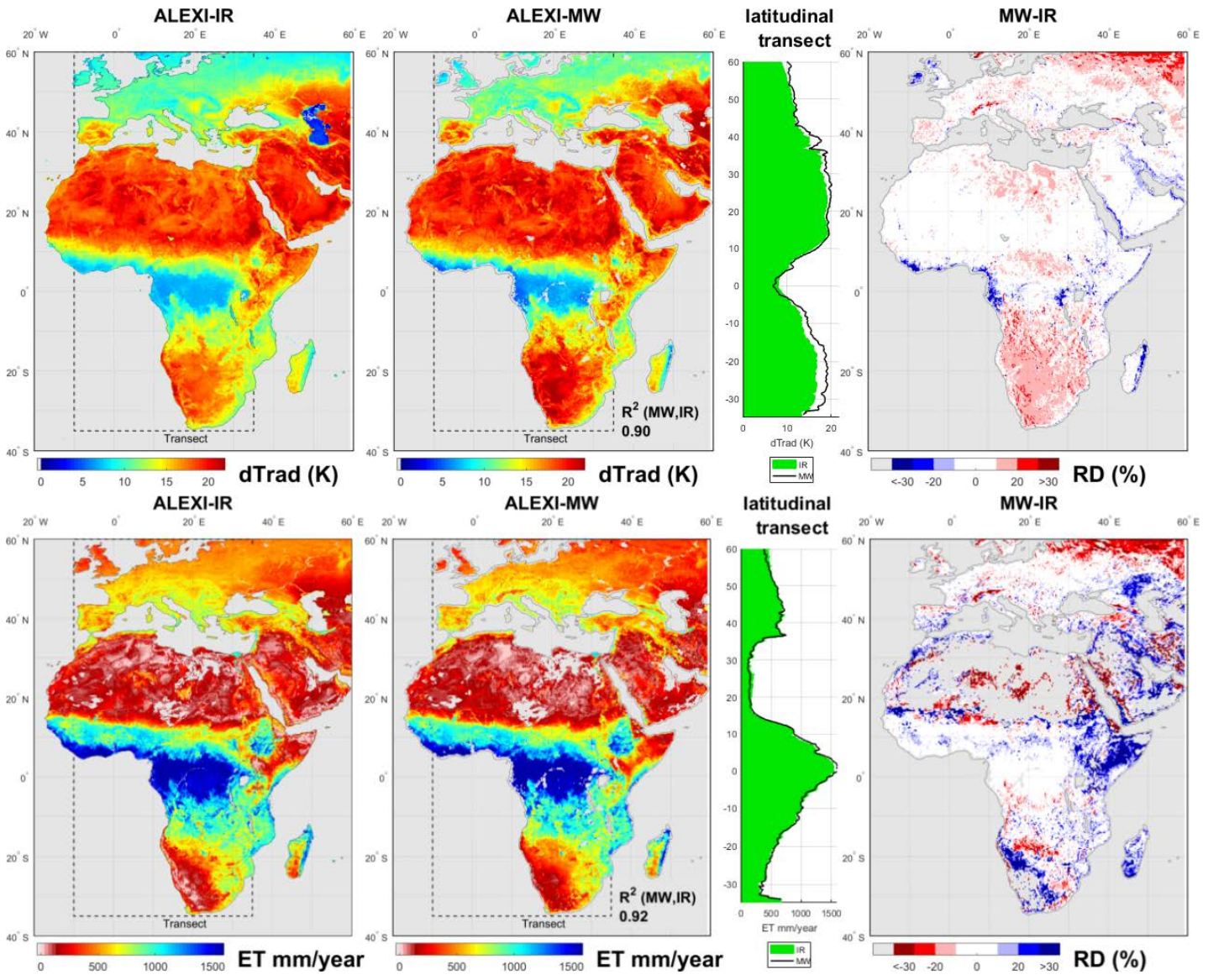

Figure 4: Multi-year mean of clear-sky ΔT_{rad} (top row, 2004-2011) and mean annual clear-sky ET (bottom row, 2003-2011) for IR and MW. The transect shows the latitudinal average for longitude 10°W to 35°E. The right-hand panel shows the corresponding relative difference (RD) between the two estimates (MW - IR), with areas with ET below 14 mm/month greyed out. Note the reversed colour bars for ΔT_{rad} and ET to emphasize their negative correlation (ΔT_{rad} up, ET down). ΔT_{rad} is defined in the ALEXI framework as the temperature rise between 1.5 hr after sunrise to 1.5 hr before noon (see Section 2.1).

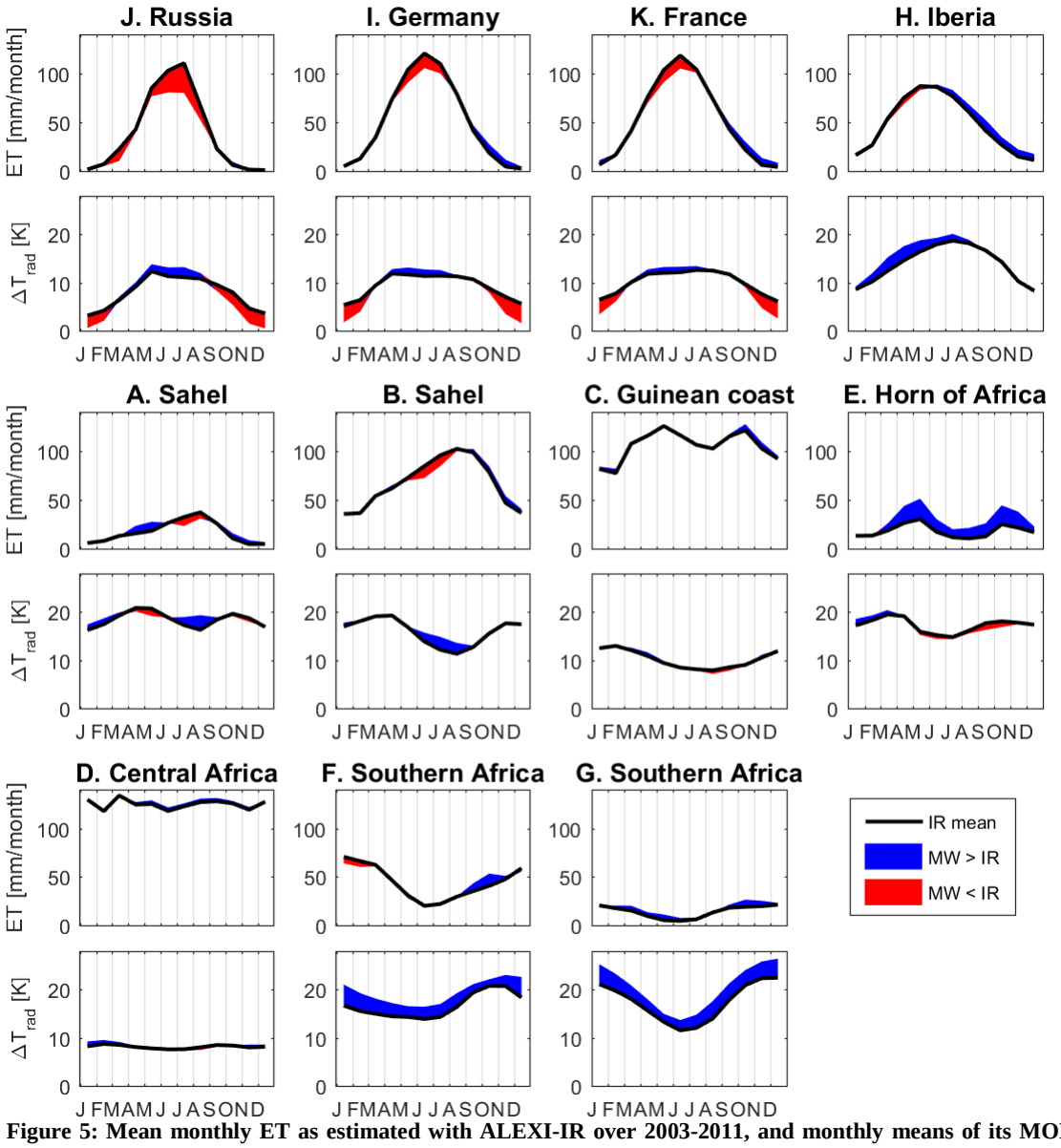

Figure 5: Mean monthly ET as estimated with ALEXI-IR over 2003-2011, and monthly means of its MODIS-based ΔT_{rad} input (period 2004-2011), for selected regions. The deviation from these IR estimates when using the MW inputs is shown in blue for a positive deviation and red for a negative deviation.

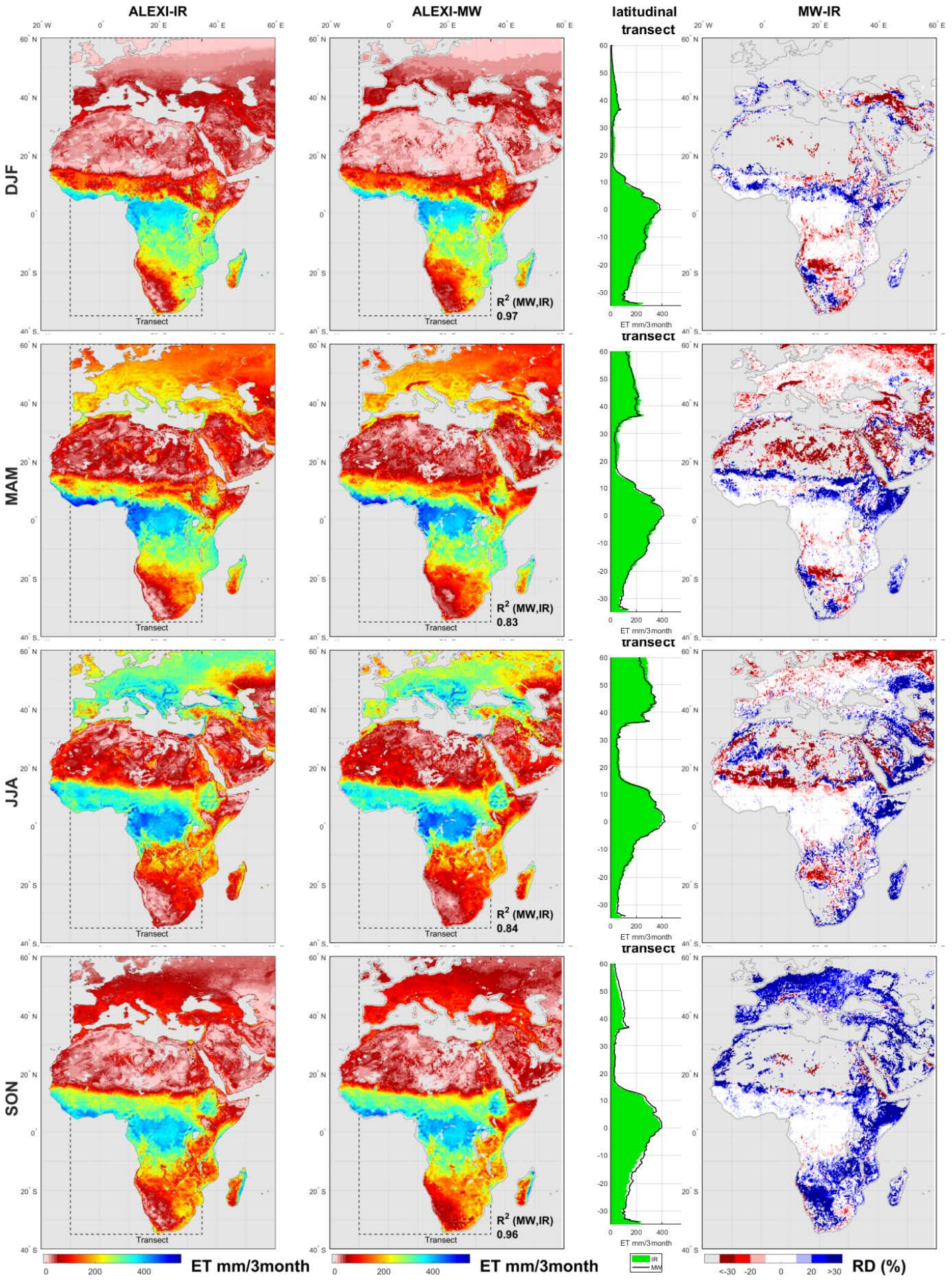
ALEXI-IR
ALEXI-MW
latitudinal transect
MW-IR
DJF
MAM
JJA
SON
Transect
R2 (MW,IR)
0.97
0.83
0.84
0.96
ET mm/3month
RD (%)
IR
MW

Figure 6: As Fig 4, but now averaged by season.

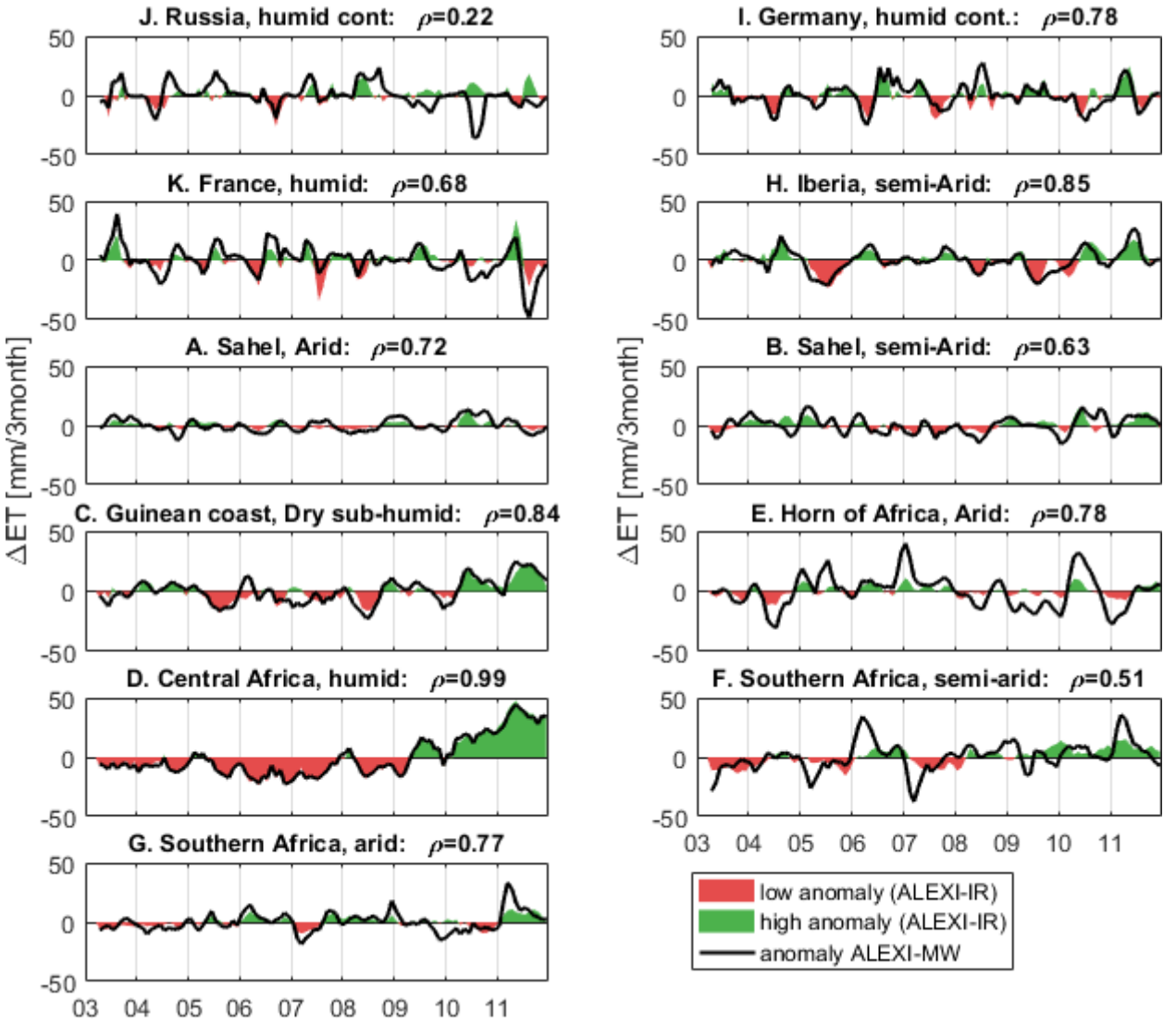

Figure 7: Comparison of anomaly in 3-month ET totals as calculated from ALEXI-IR and ALEXI-MW for selected regions (see Fig. 3 for definition of regions).

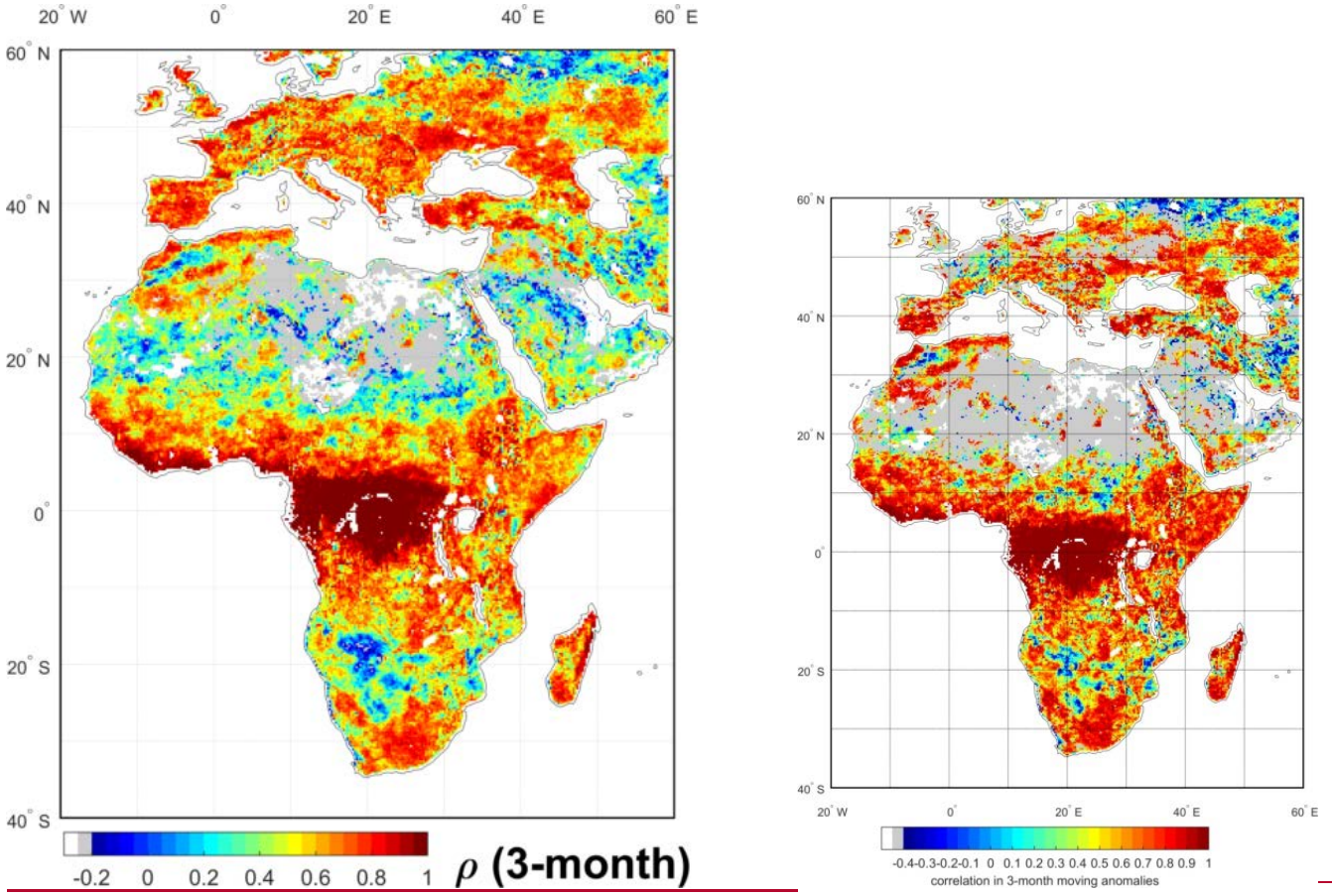

Figure 8: Pearson's correlation between anomaly in 3-month ET totals as estimated by ALEXI-IR and ALEXI-MW, calculated at 0.25 degree resolution. White areas have no data, grey areas are masked because the standard deviation in 3-month anomaly was below ~~17~~ 8 mm/3month in both estimates.

5

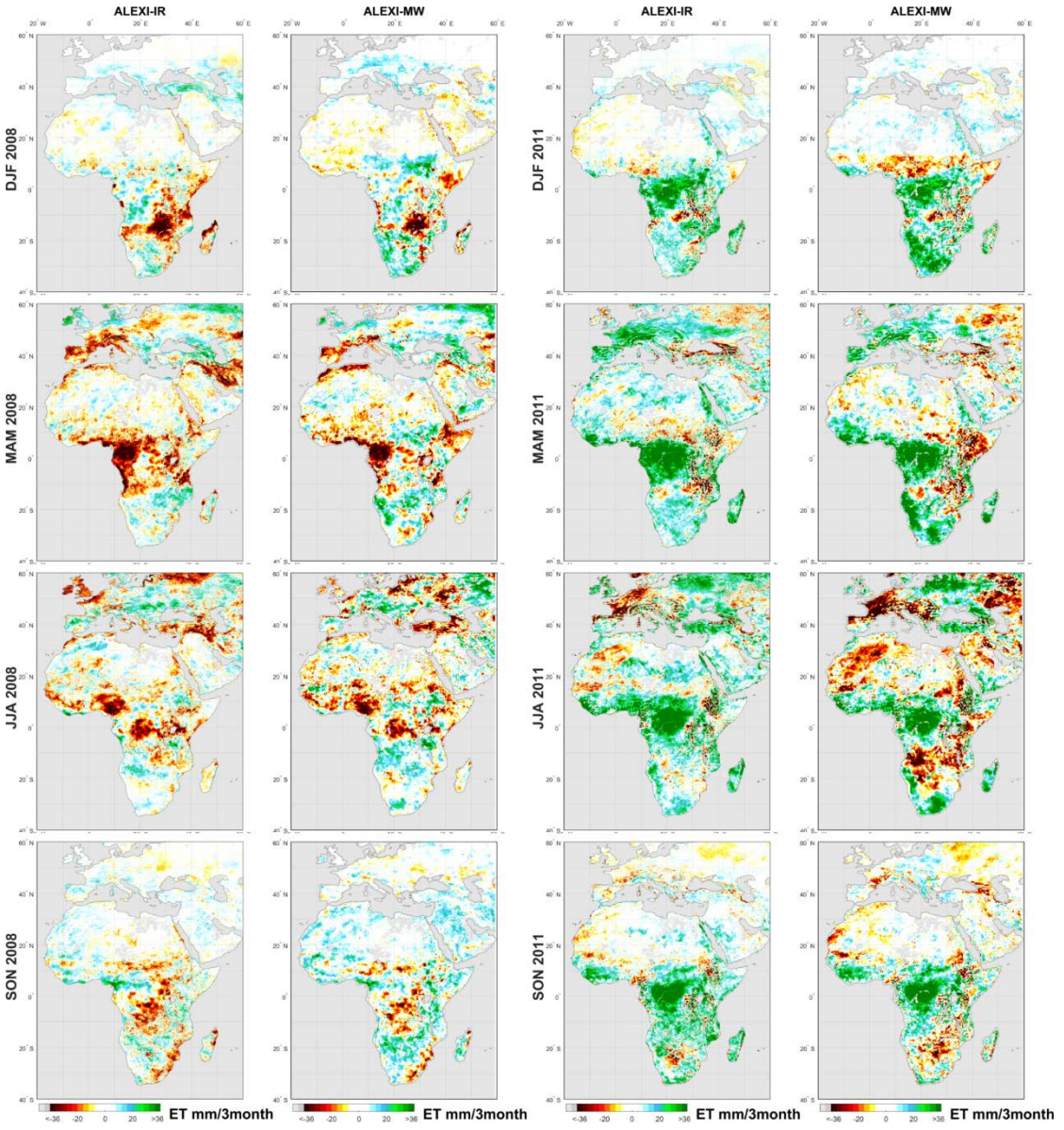

Figure 9: Anomaly in seasonal ET compared to multi-year mean (2003-2011, see Fig 6) as retrieved by ALEXI-IR and ALEXI-MW. The first two columns show the anomalies for 2008 and the two right-hand columns show them for 2011.

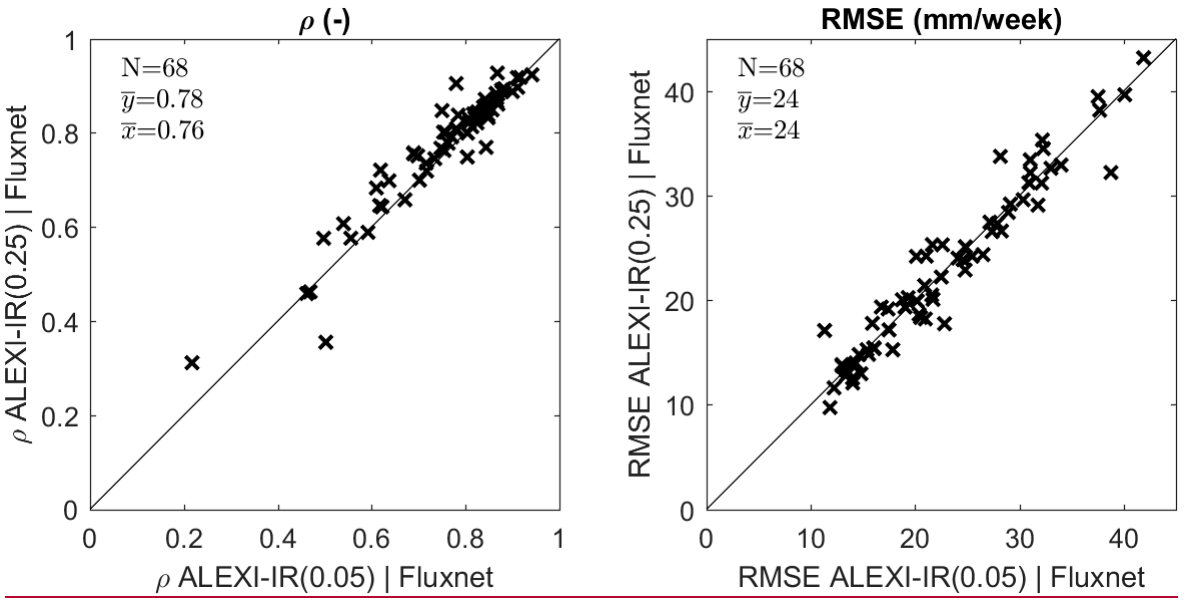

Figure 10: The effect of spatial resolution in satellite product on Pearson correlation (ρ) and RMSE between weekly ET estimates from satellite data (ALEXI-IR) and flux-tower eddy-covariance measurements (Fluxnet). Each marker represents a single station and compares results at the original 0.05° resolution of ALEXI-IR (X-axis) with those calculated for 0.25° resolution ALEXI-IR (Y-axis).

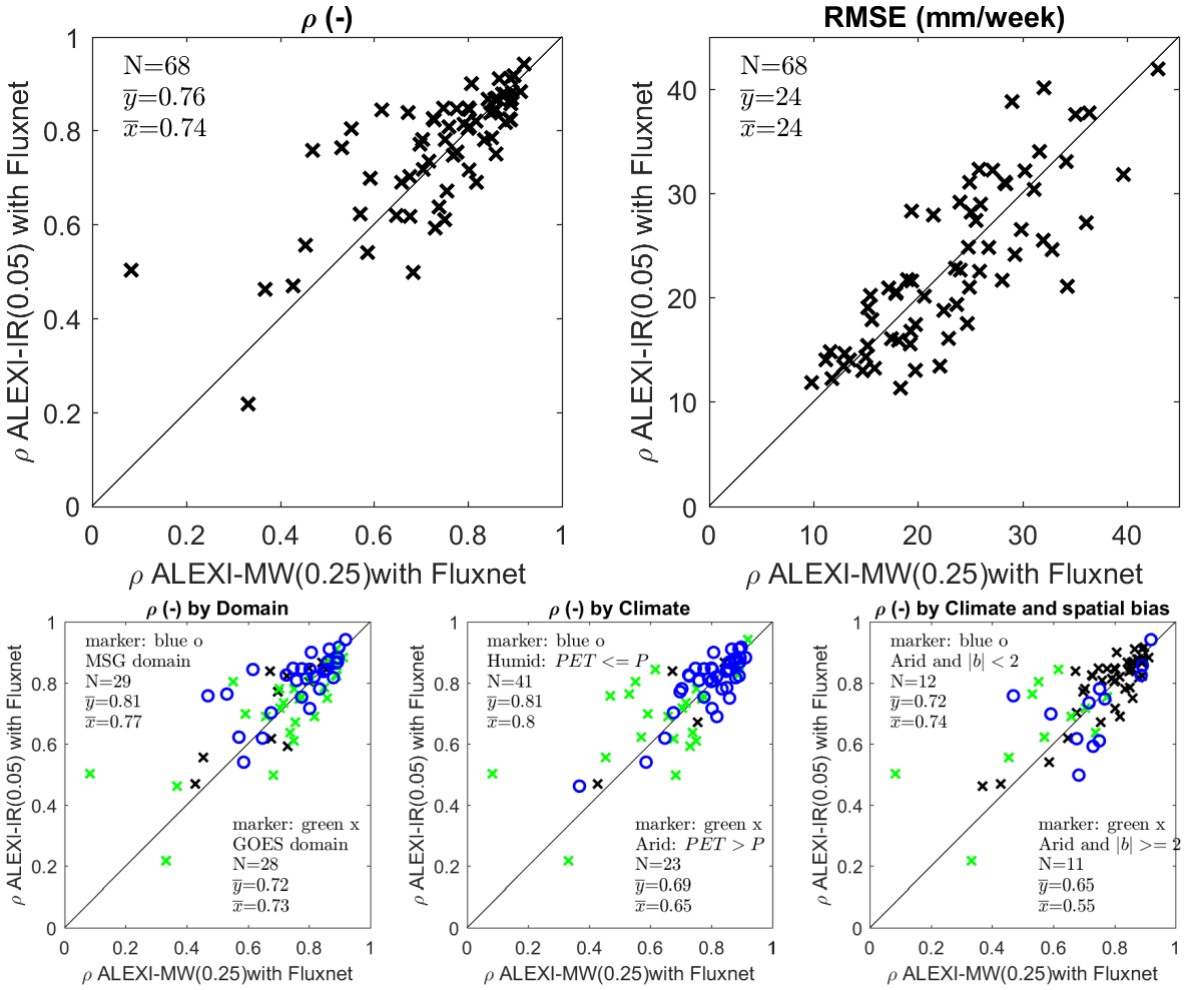
ρ (-)
N=68
$\overline{y}$=0.76
$\overline{x}$=0.74
ρ ALEXI-IR(0.05) with Fluxnet
ρ ALEXI-MW(0.25)with Fluxnet
RMSE (mm/week)
N=68
$\overline{y}$=24
$\overline{x}$=24
ρ ALEXI-IR(0.05) with Fluxnet
ρ ALEXI-MW(0.25)with Fluxnet
ρ (-) by Domain
marker: blue o
MSG domain
N=29
$\overline{y}$=0.81
$\overline{x}$=0.77
marker: green x
GOES domain
N=28
$\overline{y}$=0.72
$\overline{x}$=0.73
ρ (-) by Climate
marker: blue o
Humid: $PET <= P$
N=41
$\overline{y}$=0.81
$\overline{x}$=0.8
marker: green x
Arid: $PET > P$
N=23
$\overline{y}$=0.69
$\overline{x}$=0.65
ρ (-) by Climate and spatial bias
marker: blue o
Arid and $|b| < 2$
N=12
$\overline{y}$=0.72
$\overline{x}$=0.74
marker: green x
Arid and $|b| >= 2$
N=11
$\overline{y}$=0.65
$\overline{x}$=0.55

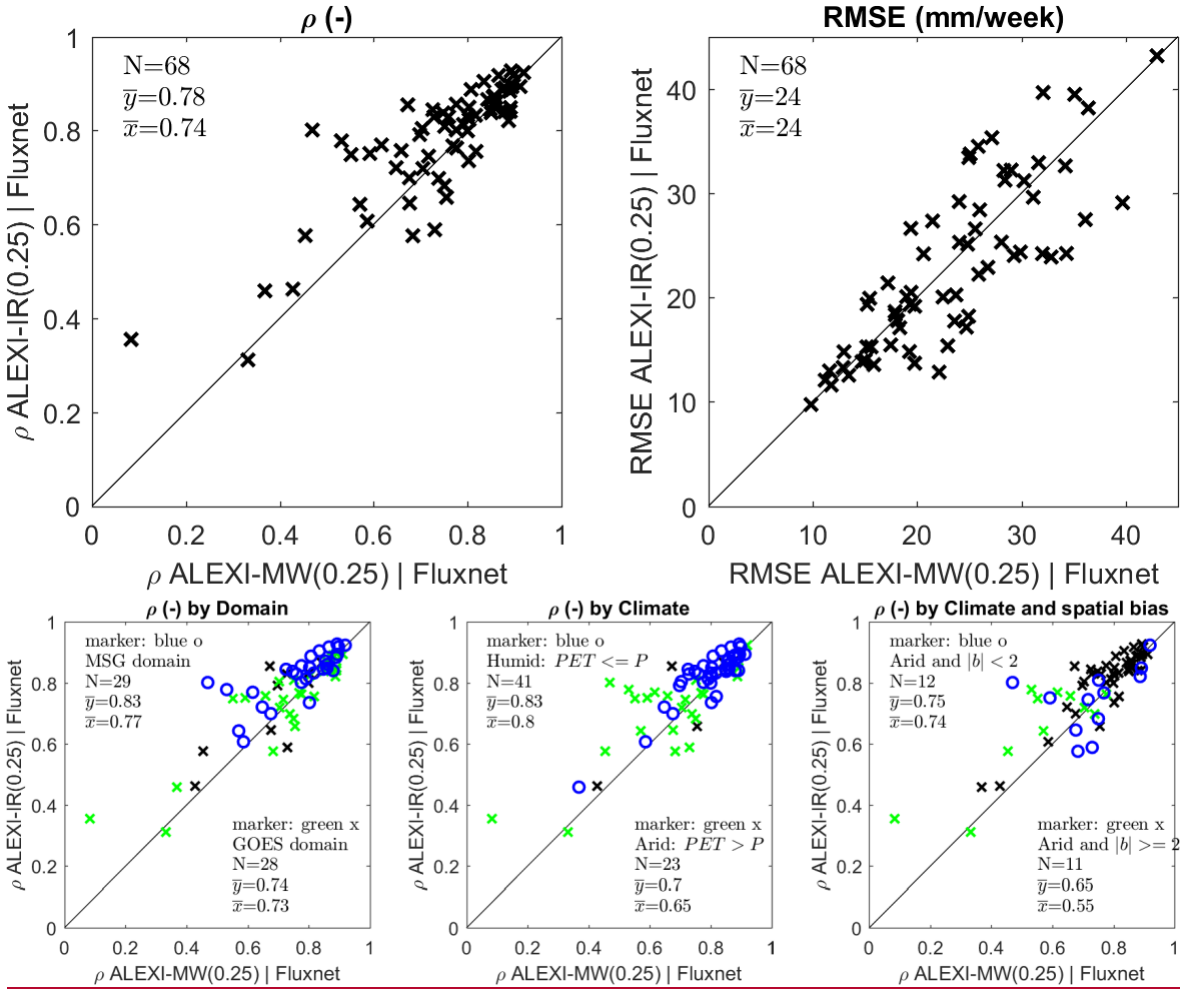

Figure 1~~0~~: The effect of switching from TIR to MW-LST as input to ALEXI on Pearson correlation (ρ) and RMSE between weekly ALEXI ET estimates and flux-tower eddy-covariance measurements (Fluxnet). Each marker represents a single station and compares results calculated for ALEXI-MW (X-axis) with those calculated for ALEXI-IR (Y-axis).

~~**Comparison of Pearson correlation (ρ) and RMSE between satellite data and Fluxnet observations. Top row: comparison between ALEXI-MW (X-axis) and ALEXI-IR (Y-axis).**~~ **Second row: same data as presented in the left-hand panel on the top row, but now distinct subsets of the tower sites are emphasized. The first panel splits the sites by geographic region, the second panel based on climate (Humid Vs Arid, see text for definition). Panel three splits the 'arid' sites further based on bias between the ALEXI-IR (0.05°) and the mean value for the encompassing 0.25° grid box with a threshold of |b|=2mm/week. The black x mark stations that are either below 60°N, or are not covered by the two contrasting selections.**

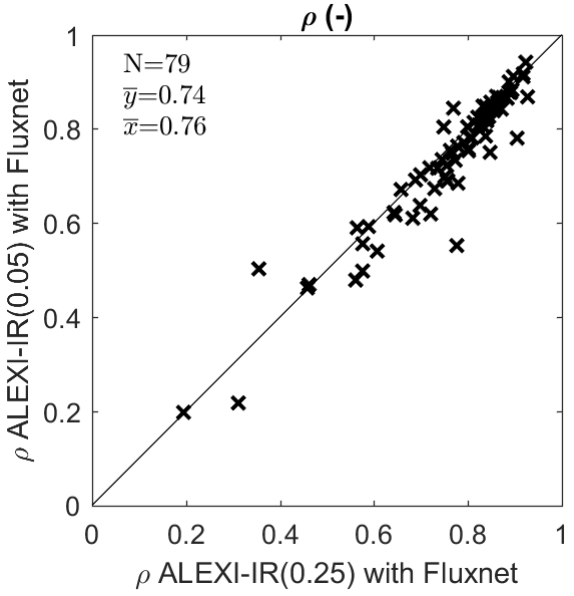

~~**Figure 11: Same as Fig 10, top left hand panel, but now showing the effect of spatial resolution by comparing the Pearson correlation of the original ALEXI IR(0.05°) with tower data (Y-axis), with that of ALEXI IR(0.25°) and tower data (Y-axis).**~~

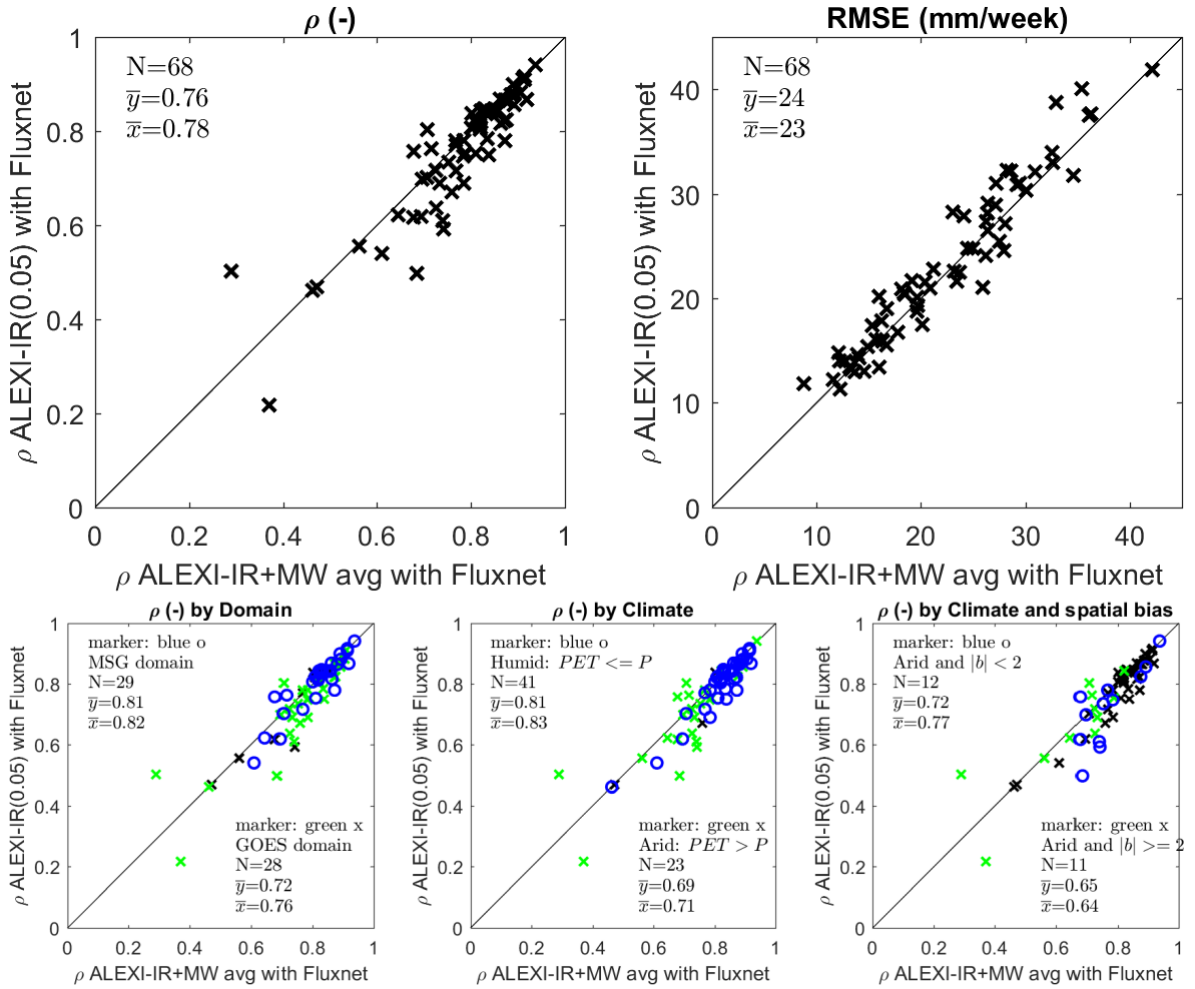

~~**Fig 12: Same as Fig 10, but now on the X-axis the temporal correspondence between Flux tower observations and ALEXI IR+MW, the average of ALEXI IR(0.05°) and ALEXI MW(0.25°).**~~